

ON FREQUENCY-DEPENDENT ROCK EXPERIMENTS: A COMPARATIVE REVIEW

Stian Rørheim*

August 7, 2022

ABSTRACT

Rock properties are environment- and condition-dependent which render field-laboratory comparisons ambiguous for a number of known and unknown reasons that constitute the upscaling problem. Unknowns are first transformed into knowns in a controlled environment (laboratory) and second in a volatile environment (field). Causality-bound dispersion and attenuation are respectively defined as rock properties that are frequency- and distance-dependent: dispersion implies non-zero attenuation and vice versa. Forced-Oscillation (FO), Resonant Bar (RB), and Pulse-Transmission (PT) are the customary techniques to measure rock properties at Hz, kHz, and MHz frequencies. Notably FO has emerged as the current champion in bridging the field-laboratory void in recent years. Not only is FO probing seismic (Hz) frequencies but with $\sim 10^{-6}$ strain amplitudes it is also similar to field seismic. RB and PT are concisely however FO is verbosely elaborated by chronologically compiling most (if not all) FO studies on sedimentary rocks and comparing all available FO measurements on reference materials such as lucite, aluminium, and PEEK. First of its kind, this inter-laboratory comparison may serve as a reference for others who seek to verify their own results. Differences between FO are discussed with alternative strain and stress sensors being the focal points. Other techniques such as Resonant Ultrasound Spectroscopy (RUS), Laser UltraSonics (LUS), and Differential Acoustic Resonance Spectroscopy (DARS) that are similar to FO, RB, and PT are also described. Only time will tell what the future holds for FO but plausible improvements for the future are ultimately given which may elevate it even further.

Key words: Dispersion; Attenuation; Forced-Oscillation; Resonant Bar; Pulse-Transmission.

*Norwegian University of Science and Technology (NTNU), Trondheim, Norway.

1 INTRODUCTION

Laboratory and field measurements are not easily compared for a number of known and unknown reasons that constitute the upscaling problem. These measurements are based on wave reflection and refraction (field) or transmission and to some extent echo (laboratory). Due to the dispersive (frequency-dependent) nature of fluid-saturated rocks, traditional laboratory (MHz) and field (Hz and kHz) measurements are incompatible. Dispersion is both a laboratory and field phenomenon that occurs whenever properties measured at different frequencies are compared. For example, White et al. [1] inadvertently described dispersion from seismic to sonic field data while studying anisotropy. Caution must thus be exercised when comparing data or basing models (measured or valid at certain frequencies) on dispersive parameters (measured at other frequencies). Attenuation effects are included in many algorithms for waveform modeling, imaging, and full-waveform inversion among other field-relevant applications. Experimental studies in controlled conditions are paramount to universally understand this fluid-related phenomenon and its mechanisms.

Forced-Oscillation (FO), Resonant Bar (RB), and Pulse-Transmission (PT) are three common techniques to measure rock properties at seismic (Hz), sonic (kHz), and ultrasonic (MHz) frequencies, respectively. Particularly FO and to some extent also RB are increasingly recognized as means to cover seismic and sonic frequencies (from Hz to kHz) in the laboratory. These techniques share the common denominator that all were first used to study metals by physicists but were later adopted by rock physicists to also study rocks. Progress is inevitable as the number of laboratory studies at similar frequencies as in the field are rapidly increasing despite measuring dissimilar parameters. In fact, also the measured parameters are environment-dependent. For example, FO in its basic (longitudinal) form measures Young's modulus and Poisson's ratio instead of P- and S-wave velocities at seismic frequencies, while its auxiliary (uniaxial) form measures uniaxial modulus equivalent to P-wave velocity. Transformation between moduli and velocities inevitably introduces errors despite being trivial for isotropic and non-trivial for anisotropic rocks. FO novelty is driven by extending the frequencies at which it operates, what properties it measures and how in terms of sensor types, improving its boundary conditions (dead volume), and recently also its concurrent imaging via CT.

This study is in its entirety based on Rørheim [4] but with minor modifications for formatting purposes. Rørheim [5] was its first iteration and Rørheim and Holt [6] its second but it has since been expanded into greater detail while being continuously updated to keep up with time as novel experiments are becoming customary. In fact, unknown to Rørheim [5] at the time, Subramaniyan et al. [7] is an excellent review of apparatuses with the ability to measure seismic attenuation in reservoir rocks. Similarities between this study and Subramaniyan et al. [7] are evident as both are inter-laboratory comparisons however the focus of Subramaniyan et al. [7] was on the standardization need of FO apparatuses whereas the present is on comparing FO measured moduli and attenuations on lucite, aluminum, and PEEK reference specimens. Subramaniyan et al. [7] did not cover all apparatuses and only considered reservoir rocks such as sandstones and carbonates unlike unconventional ones like shale. Validating attenuation measurements by literature comparison was the basis of Rørheim and Holt [6]. Like Subramaniyan et al. [7], the three most common techniques (FO, RB, and PT) are the focal points (FO more so than RB and PT), but unlike Subramaniyan et al. [7], other novel techniques such as Resonant Ultrasound Spectroscopy (RUS), Differential Acoustic Resonance Spectroscopy (DARS), and Laser UltraSonics (LUS) are also elaborated. The primary three techniques (FO, RB, and PT) are also theoretically defined whereas the secondary ones (RUS, DARS, and LUS) are not. Recent numerical advances are also included as the value and significance of Digital Rock Physics (DRP) surely will improve in the future when elevated from its current infancy.

2 THEORY

RB, PT, and FO are related due to all three exploiting mechanical disturbances in a material to deduce its properties. Here the theory of FO is elaborated while that of RB and PT are mostly unelaborated due to FO being the primary focus from the outset and throughout. Relevant models commonly used to simulate the dispersive (or frequency-dependent) behaviour of rocks across frequencies are also briefly explained.

2.1 MECHANICAL EQUATIONS

RB exploits harmonic waves in the axial direction with radial u_r , circumferential u_θ , and axial u_z components of displacement. z -dependent but θ -independent motions are separated into torsional waves with u_θ and longitudinal waves with u_r and u_z . Flexural waves are z - and θ -dependent motions. Phase velocities V at resonating frequencies f relate to bar length L as

$$V = \underbrace{\frac{2L}{n}}_{\lambda} f, \quad (1)$$

where $n \in \{1, 2, 3, \dots\}$ denotes different modes or harmonics and λ is the wavelength. $n = 1$ is the fundamental frequency. Young's modulus E from longitudinal and flexural modes is $E = \rho V_E^2$, whereas shear modulus G from the torsional mode is $G = \rho V_G^2$, with V_E , V_G , and ρ being longitudinal or flexural velocity, torsional velocity, and density [8]. PT exploits the time of flight principle to determine P- and S-wave velocities

$$V = \frac{L}{\Delta t}, \quad (2)$$

where V is the velocity of either body wave type, L is the specimen length, and Δt is the travel time (Figure 1a). FO measures different moduli and ratios depending on excitation modes: (i) longitudinal, (ii) torsional, (iii) flexural, (iv) volumetric, and (i) uniaxial. Elastic moduli are generally defined as stress over strain $M \equiv \sigma/\epsilon$. (i) yields Young's modulus and Poisson's ratio ν respectively as

$$E = \frac{\sigma_{\mathbf{ax}}}{\epsilon_{\mathbf{ax}}}, \quad (3)$$

$$\nu = -\frac{\epsilon_{\mathbf{rad}}}{\epsilon_{\mathbf{ax}}}, \quad (4)$$

with σ and ϵ being stress and strain either in **ax**(ial) or **rad**(ial) direction (Figure 1b). (ii) provides shear modulus G as the shear stress-strain ratio

$$G = \frac{\sigma_s}{\epsilon_s}, \quad (5)$$

in which σ_s and ϵ_s are shear stress and shear strain, respectively. Kelvin [9] regarded K and G as principal elasticities with special significance. (iii) adds flexural modulus E_F but remains undefined due to its condition-dependent definitions. Flexural and Young's moduli are theoretically equivalent $E = E_F$ but practically inequivalent $E \neq E_F$. (iv) grants bulk modulus K as the three-dimensional extension of Young's modulus E . It is defined as an object's proclivity to deform in all directions under hydrostatic stress or pressure regimes

$$K = \frac{\sigma_p}{\epsilon_{\text{vol}}}, \quad (6)$$

where σ_p (or P_p) is hydrostatic stress (or pressure) and ϵ_{vol} is volumetric strain. (v) gives uniaxial (or P-wave) modulus H which is akin to Young's modulus E but for $\epsilon_{rad} = 0$ enforcing uniaxial-strain instead of uniaxial-stress conditions (Figure 1c)

$$H = \left. \frac{\sigma_{ax}}{\epsilon_{ax}} \right|_{\epsilon_{rad}=0}. \quad (7)$$

Lamé's λ_L and μ_L [10] parameterize $K = \lambda_L + 2/3\mu_L$ where $\mu_L = G$ and λ_L is physically equivocal. P- and S-wave velocities V_P and V_S are then

$$V_P = \sqrt{\frac{K + \frac{4}{3}G}{\rho}} = \sqrt{\frac{\lambda_L + 2\mu_L}{\rho}},$$

$$V_S = \sqrt{\frac{G}{\rho}} = \sqrt{\frac{\mu_L}{\rho}},$$

whereas $V_P/V_S = \sqrt{K/G + 4/3} = \sqrt{\lambda_L/\mu_L + 2}$ is density-independent.

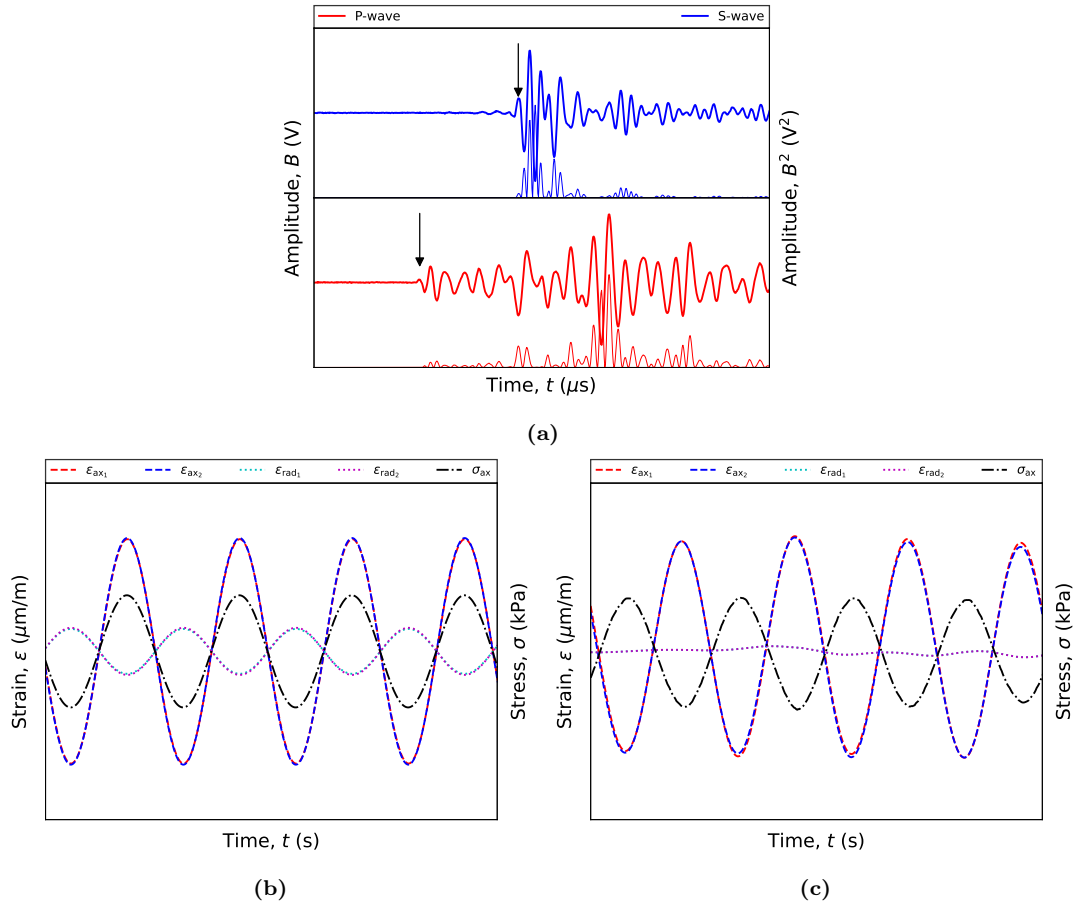


Figure 1 Amplitudes B , ϵ , and σ versus time t exemplified for three different techniques: (a) PT and two FO versions: uniaxial-stress (b) and uniaxial-strain (c). Arrows in (a) indicate first maxima.

2.1.1 ISOTROPY VERSUS ANISOTROPY

Anisotropic or isotropic is the medium whose elastic properties change or unchange with direction. Hookean theory [11, 12] first formulated as “ut tensio, sic vis”¹ relates stress σ_{ij} and strain ϵ_{kl} as $\sigma_{ij} = \sum_{k=1}^3 \sum_{l=1}^3 C_{ijkl} \epsilon_{kl}$ where C_{ijkl} is stiffness and $i, j = 1, 2, 3$ using Einstein notation [13]. Transforming between E , ν , G , K , and H is isotropically trivial (Table 1) yet anisotropically non-trivial as the number of specimens and stiffnesses required for full description increases from one (Figure 2) to three (Figure 3) and from two (Equation 8) to five (Equation 9) using Voigt notation [14] for Transverse Isotropy (TI), respectively. Stress $\vec{\sigma} = (\sigma_{11} \sigma_{22} \sigma_{33} \sigma_{23} \sigma_{13} \sigma_{12}) \equiv (\sigma_1 \sigma_2 \sigma_3 \sigma_4 \sigma_5 \sigma_6)$ and strain $\vec{\epsilon} = (\epsilon_{11} \epsilon_{22} \epsilon_{33} \epsilon_{23} \epsilon_{13} \epsilon_{12}) \equiv (\epsilon_1 \epsilon_2 \epsilon_3 \epsilon_4 \epsilon_5 \epsilon_6)$ combined with $\vec{C} = C_{ij}$ denoting either two stiffnesses C_{11} and C_{44} describe isotropic rocks as

$$\underbrace{\begin{pmatrix} \sigma_{11} \\ \sigma_{22} \\ \sigma_{33} \\ \sigma_{23} \\ \sigma_{13} \\ \sigma_{12} \end{pmatrix}}_{\vec{\sigma}} = \underbrace{\begin{pmatrix} C_{11} & C_{11} - 2C_{44} & C_{11} - 2C_{44} & 0 & 0 & 0 \\ C_{11} - 2C_{44} & C_{11} & C_{11} - 2C_{44} & 0 & 0 & 0 \\ C_{11} - 2C_{44} & C_{11} - 2C_{44} & C_{11} & 0 & 0 & 0 \\ 0 & 0 & 0 & C_{44} & 0 & 0 \\ 0 & 0 & 0 & 0 & C_{44} & 0 \\ 0 & 0 & 0 & 0 & 0 & C_{44} \end{pmatrix}}_{\vec{C}} \underbrace{\begin{pmatrix} \epsilon_{11} \\ \epsilon_{22} \\ \epsilon_{33} \\ 2\epsilon_{23} \\ 2\epsilon_{13} \\ 2\epsilon_{12} \end{pmatrix}}_{\vec{\epsilon}}, \quad (8)$$

or three additional stiffnesses C_{13} , C_{33} , and C_{66} describe anisotropic rocks as

$$\underbrace{\begin{pmatrix} \sigma_{11} \\ \sigma_{22} \\ \sigma_{33} \\ \sigma_{23} \\ \sigma_{13} \\ \sigma_{12} \end{pmatrix}}_{\vec{\sigma}} = \underbrace{\begin{pmatrix} C_{11} & C_{11} - 2C_{66} & C_{13} & 0 & 0 & 0 \\ C_{11} - 2C_{66} & C_{11} & C_{13} & 0 & 0 & 0 \\ C_{13} & C_{13} & C_{33} & 0 & 0 & 0 \\ 0 & 0 & 0 & C_{44} & 0 & 0 \\ 0 & 0 & 0 & 0 & C_{44} & 0 \\ 0 & 0 & 0 & 0 & 0 & C_{66} \end{pmatrix}}_{\vec{C}} \underbrace{\begin{pmatrix} \epsilon_{11} \\ \epsilon_{22} \\ \epsilon_{33} \\ 2\epsilon_{23} \\ 2\epsilon_{13} \\ 2\epsilon_{12} \end{pmatrix}}_{\vec{\epsilon}}, \quad (9)$$

where C_{11} , C_{13} , C_{33} , C_{44} , and C_{66} combinations yield the anisotropic versions of E , ν , G , K , and H . For example, without further elaboration, isotropic E and ν expand to anisotropic E_V , E_{45} , and E_H as well as ν_{VH} , ν_{HV} , and ν_{HH} for the longitudinal mode, while $H = C_{33}$ in Equation 7 for the uniaxial mode of a 0° specimen.

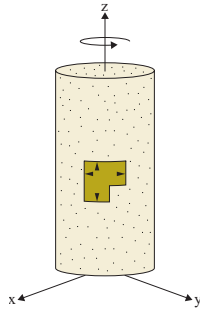


Figure 2 Geometry of an isotropic specimen. Triangles indicate measurement directions of biaxial strain gauges.

¹“As the extension, so the force” is Hooke’s 1678 solution [11] to his 1675 anagram “ceiinnosssttuu” [12].

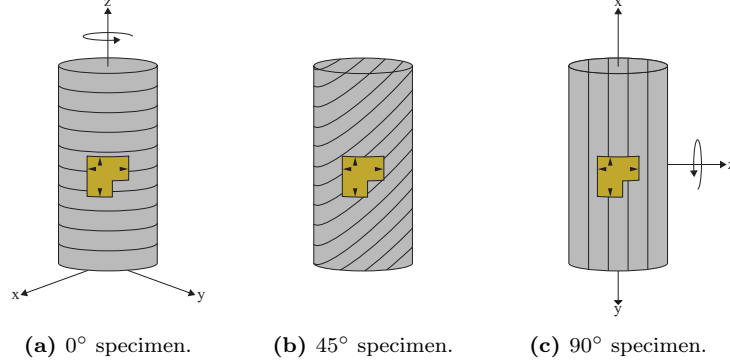


Figure 3 Geometries of (a) 0, (b) 45, and (c) 90° specimens assuming TI symmetry. Triangles indicate measurement directions of biaxial strain gauges.

2.2 ATTENUATION EQUATIONS

Frequency-dependent rock behaviour caused by wave-induced fluid motions at different scales within the porous network is related to the causal-consistent dispersion and attenuation phenomena. The quality factor Q is a measure of a material's dissipativity [15]. “The greater the value of Q , the smaller the internal friction” [18] which is intuitive since, vice versa, low Q -values imply large dissipations. Q or Q^{-1} customarily describes attenuation and comes in many forms including as the imaginary M_{\Im} and real M_{\Re} parts of complex modulus M [19]

$$Q^{-1} = \frac{M_{\Im}}{M_{\Re}} \quad (10)$$

as the ratio of energy stored W_m to energy loss per cycle ΔW [20]

$$Q^{-1} = \frac{\Delta W}{2\pi W_m}, \quad (11)$$

or as the tangent of the phase angle $\Delta\theta$ between the applied stress θ_σ and the resulting strain θ_ϵ [21]

$$Q^{-1} = \tan \underbrace{\overbrace{\theta_{\text{STD}}^{\theta_\sigma} - \theta_{\text{SPE}}^{\theta_\epsilon}}^{\Delta\theta}}, \quad (12)$$

which in practice corresponds to the phase angle $\Delta\theta$ between the standard θ_{STD} and the specimen θ_{SPE} exemplified by Figure 4. Equation 12 is particularly useful for FO, whereas RB and PT respectively rely on the width of the resonant peak or the time constant of the resonant decay and the Spectral Ratio (SR) method to determine Q . Morozov [22] questioned the usefulness of Q as a measure and if its many definitions are “true”, “assumed”, or “apparent”.

To evaluate mechanisms, Winkler and Nur [23] assumed an isotropic solid described by complex moduli with small imaginary parts to transform between two moduli

$$\frac{(1-\nu)(1-2\nu)}{Q_P} = \frac{1+\nu}{Q_E} - \frac{2\nu(2-\nu)}{Q_G}, \quad (13a)$$

Table 1 Tabulated relationships among elastic constants in an isotropic material modified from Mavko et al. [15] who based it on Birch [16]. Similar tabulated versions of these relations are common in literature (even Gassmann [17] included one). Given any combination of two parameters, any other elastic properties are uniquely determined from these formulae. The last row features the relationship as functions of velocities V_P and V_S as well as density ρ . The last column features V_P/V_S described by different pairs of elastic constants.

Parameters	K	E	λ_L	ν	H	μ_L	V_P/V_S
(λ_L, μ_L)	$\lambda_L + \frac{2}{3}\mu_L$	$\mu_L \left(\frac{3\lambda_L + 2\mu_L}{\lambda_L + \mu_L} \right)$		$\frac{\lambda_L}{2(\lambda_L + \mu_L)}$	$\lambda_L + 2\mu_L$		$\left(\frac{\lambda_L + 2\mu_L}{\mu_L} \right)^{\frac{1}{2}}$
(K, λ_L)		$9K \left(\frac{K - \lambda_L}{3K - \lambda_L} \right)$		$\frac{\lambda_L}{3K - \lambda_L}$	$3K - 2\lambda_L$	$\frac{3(K - \lambda_L)}{2}$	$\left(\frac{\frac{4}{3}\lambda_L - 2K}{\lambda_L - K} \right)^{\frac{1}{2}}$
(K, μ_L)		$\frac{9K\mu_L}{3K + \mu_L}$	$K - \frac{2}{3}\mu_L$	$\frac{3K - 2\mu_L}{2(3K + \mu_L)}$	$K + \frac{4}{3}\mu_L$		$\left(\frac{K + \frac{4}{3}\mu_L}{\mu_L} \right)^{\frac{1}{2}}$
(E, μ_L)	$\frac{E\mu_L}{3(3\mu_L - E)}$		$\mu_L \left(\frac{E - 2\mu_L}{3\mu_L - E} \right)$	$\frac{E}{2\mu_L} - 1$	$\mu_L \left(\frac{4\mu_L - E}{3\mu_L - E} \right)$		$\left(\frac{E - 4\mu_L}{E - 3\mu_L} \right)^{\frac{1}{2}}$
(K, E)			$3K \left(\frac{3K - E}{9K - E} \right)$	$\frac{3K - E}{6K}$	$3K \left(\frac{3K + E}{9K - E} \right)$	$\frac{3KE}{9K - E}$	$\left(\frac{E + 3K}{E} \right)^{\frac{1}{2}}$
(λ_L, ν)	$\lambda_L \left(\frac{1+\nu}{3\nu} \right)$	$\lambda_L \frac{(1+\nu)(1-2\nu)}{\nu}$			$\lambda_L \left(\frac{1-\nu}{\nu} \right)$	$\lambda_L \left(\frac{1-2\nu}{2\nu} \right)$	$\left[\frac{2(1-\nu)}{(1-2\nu)} \right]^{\frac{1}{2}}$
(μ_L, ν)	$\nu \left[\frac{2(1+\nu)}{3(1-2\nu)} \right]$	$2\mu_L(1+\nu)$	$\mu_L \left(\frac{2\nu}{1-2\nu} \right)$		$\mu_L \left(\frac{2-2\nu}{1-2\nu} \right)$		$\left[\frac{2(1-\nu)}{(1-2\nu)} \right]^{\frac{1}{2}}$
(K, ν)		$3K(1-2\nu)$	$3K \left(\frac{\nu}{1+\nu} \right)$		$3K \left(\frac{1-\nu}{1+\nu} \right)$	$3K \left(\frac{1-2\nu}{2+2\nu} \right)$	$\left[\frac{2(1-\nu)}{(1-2\nu)} \right]^{\frac{1}{2}}$
(E, ν)	$\frac{E}{3(1-2\nu)}$		$\frac{E\nu}{(1+\nu)(1-2\nu)}$		$\frac{E(1-\nu)}{(1+\nu)(1-2\nu)}$	$\frac{E}{2(1+\nu)}$	$\left[\frac{2(1-\nu)}{(1-2\nu)} \right]^{\frac{1}{2}}$
(H, ν)	$H - \frac{4}{3}\mu_L$	$\mu_L \left(\frac{3H - 4\mu_L}{H - \mu_L} \right)$	$H - 2\mu_L$	$\frac{H - 2\mu_L}{2(M - \mu_L)}$			$\left(\frac{H}{\mu_L} \right)^{\frac{1}{2}}$
(V_P, V_S)	$\rho \left(V_P^2 - \frac{4}{3}V_S^2 \right)$	$\rho V_S^2 \left(\frac{3V_P^2 - 4V_S^2}{V_P^2 - V_S^2} \right)$	$\rho(V_P^2 - 2V_S^2)$	$\frac{H - 2\mu_L}{2(V_P^2 - V_S^2)}$	ρV_P^2	ρV_S^2	

$$\frac{1-2\nu}{Q_K} = \frac{3}{Q_E} - \frac{2(\nu+1)}{Q_G}, \quad (13b)$$

$$\frac{1+\nu}{Q_K} = \frac{3(1-\nu)}{Q_P} - \frac{2(1-2\nu)}{Q_G}, \quad (13c)$$

with $Q_E = E_{\mathcal{R}}/E_{\mathcal{I}}$, $Q_K = K_{\mathcal{R}}/K_{\mathcal{I}}$, and $Q_G = G_{\mathcal{R}}/G_{\mathcal{I}}$ while simultaneously proving that one of these attenuation relations must be true

$$Q_K > Q_P > Q_E > Q_G, \quad (14a)$$

$$Q_K < Q_P < Q_E < Q_G, \quad (14b)$$

$$Q_K = Q_P = Q_E = Q_G. \quad (14c)$$

Johnston et al. [24] summarized a series of Q -dependencies based on the accumulation of individual attenuation measurements (frequency, strain amplitude, fluid saturation, pressure and stress, and temperature) and elaborated on attenuation mechanisms: (i) matrix anelasticity, (ii) viscosity and flow of saturating fluids, and (iii) scattering from inclusions. Mechanism (i) is related to solid friction between grains in dry rocks. Mechanism (ii) includes local Biot flow within the pore space often termed “s squirt-flow” [25], flow in heterogeneous media [26], and flow related to the wavelength-scale equilibration [27] at the respective microscopic, mesoscopic, and macroscopic scales. Mechanism (iii) tends to be significant for wavelengths close to the size of any heterogeneities. Mechanism (ii) is typically caused by Wave-Induced Fluid Flow (WIFF) [28] but evidence for Wave-Induced Gas Exsolution Dissolution (WIGED) [29] also exists. Fundamental to poroelasticity [17, 25, 30, 31] are the opposing concepts of (i) drained and (ii) undrained conditions defined as the fluid’s ability (i) or inability (ii) to flow in or out of the porous medium. Biot [27] predicted the existence of two regimes of fluid motion governed by (i) viscous effects at the low frequency limit [25] and by (ii) inertia effect at the high frequency limit [30]. Equal viscous and inertial forces of the fluid occur at Biot’s characteristic frequency while viscous flow and inertial drag respectively dominate below and above. These concepts define cut-off frequencies for the drained-undrained and quasistatic-dynamic transitions.

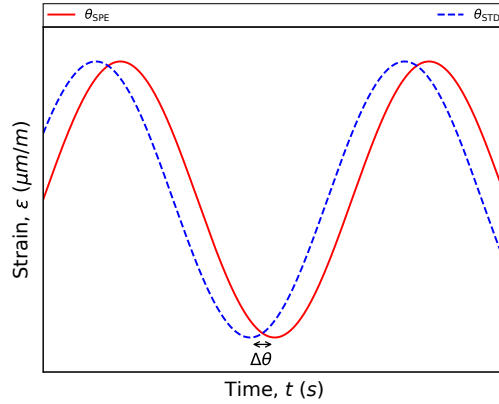


Figure 4 Equation 12 graphically displayed in which the phase shift $\Delta\theta$ between θ_{STD} and θ_{SPE} yields Q^{-1} . Both strain amplitudes are equal $B_{STD} = B_{SPE}$ for the sake of simplicity.

2.3 MODELS

“All models are wrong but some are useful”² in simulating experimental behaviour and isolating the dominant mechanisms. “Numerous theories on wave propagation exist but these concepts remain unencumbered by measured data needed to prove, delimit or extend them” [33]. An increasing number of phenomenological and non-phenomenological (predictive) models that combine flow at different scales are continuously being proposed. Since different experimental techniques cover different frequencies, models that simulate dispersive behaviour across frequencies are imperative to unite results from different experiments. Cole-Cole (CC) [34] and Standard Linear Solid (SLS) (or Zener) [35] models are among the most common ones alongside the analytical Kramers-Kronig relations (KKR) [36, 37]. CC is based on KKR and reduces to the underlying Debye model [38] if its spreading factor $\alpha \in [0, 1]$ becomes $\alpha = 0$, while SLS is based on the Maxwell [39] and Kelvin-Voigt [40, 41] models but with different combinations of springs and dashpots to represent elastic and viscous components, respectively. Burgers viscoelastic model [42] is a combination of the other models (Maxwell, Kelvin-Voigt, and Zener). KKR are the bidirectional mathematical solutions to the problem of connecting the real and imaginary parts of any complex function that is constrained by causality and analytic in the upper half-plane. Spencer [21] extended the frequency-dependent CC model from the realm of the dielectric constant of liquids to the realm of the real and imaginary parts of porous media moduli impacted by relaxation processes. Mikhaltsevitch et al. [43] considered an isotropic viscoelastic material regarded as a dynamic system for which the stress-strain relationship is linear with given mechanical properties as a numerical solution of KKR. In general, KKR is superior to CC due to its analytical nature but necessitates mechanical and attenuation measurements at all frequencies unlike CC that can be fitted using only mechanical measurements. Rørheim [4] describes a joint-fit-based procedure based on CC that uses both mechanical and attenuation measurements as input. CC is however limited to describing one relaxation time, transition, or mechanism albeit multiple may concurrently exist.

3 MEHOTDS

Experimental determination of dynamic rock properties chronologically began with Resonant Bar (RB), Pulse-Transmission (PT), and Forced-Oscillation (FO) at the respective sonic, ultrasonic, and seismic frequencies (Figure 5). All three techniques are elaborated but FO in greatest detail with (to our knowledge) all accessible studies described and summarized.

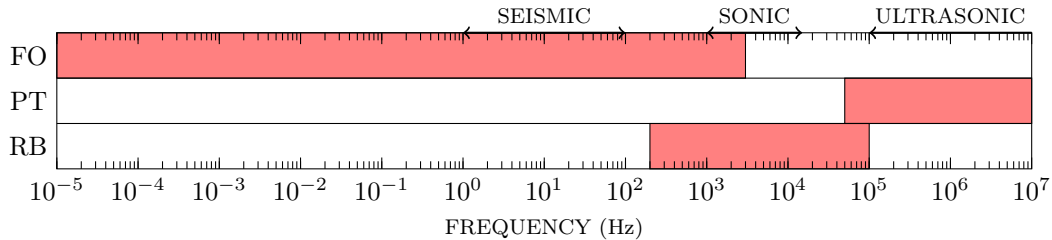


Figure 5 Probeable frequencies subdivided into seismic, sonic, and ultrasonic for the three primary techniques: RB, PT, and FO.

²Common aphorism generally attributed to Box [32].

3.1 RESONANT BAR (RB)

Ide [44] invented a technique based on Cady [45], Quimby [46], and Boyle and Sproule [47] for dynamic determination of rock properties that produced longitudinal vibrations of rods by electrostatic traction. Inspired by the novelty of their colleague’s approach, Birch and Bancroft [18] studied the longitudinal, flexural, and torsional modes of a long granite column forced into resonant vibrations excited by an alternating magnetic field. This ultimately became known as the widely acknowledged Resonant Bar (RB) technique whose function is to probe sonic frequencies. However rare measurements in the sonic frequency range may be, experiments using long and slender samples are less so than experiments involving conventional core specimens. The longer the resonator, the lower the characteristic frequency. Since frequency is lowered as a function of bar length, it is common practice to cement short length bars together due to the difficulty to directly core sufficiently long bars [48]. A sinusoidal force is traditionally submitted to one end of a rock bar fixed at its center of mass (which also coincides with the location of minimum displacement) while the resultant vibrations are measured at the other. Piezoelectric or electromagnetic transducers excite either the extensional or the torsional mode of vibration. Moduli are calculated from the resonance frequencies that depend on the material’s velocity, dimensions, and density. Attenuation is determined by the width of the resonant peak or the time constant of the resonant decay.

Despite the obvious advantage of probing sonic frequencies, Wang [49] identified (i) extensive system calibration and data corrections as well as difficulty with (ii) obtaining high-pressure, high-temperature data and (iii) pure shear mode as disadvantages. Disadvantageous is also that the characteristic frequency is a function of the bar length. Although Jones and Nur [50] extended the investigations of the effects of confining pressure, pore pressure, and degree of saturation by Winkler and Nur [51] with elevated temperatures, RB measurements at *in-situ* conditions belong to the rarities. RB suffered dimensional limitations until Tittmann [52] proposed the possibility to reduce resonance frequencies by the use of additional mass that changes the moment of inertia without altering the rigidity. These words resonated with Nakagawa [53] who realized that small specimens could be explored using a modified version of RB. Nakagawa [53] designed an apparatus geometrically similar to the Split-Hopkinson Pressure Bar (SHPB) described by Kolsky [55] and named after Hopkinson [54]. Nakagawa [53] added mass to his Split-Hopkinson Resonance Bar (SHRB) by a pair of 40.6 cm steel extension bars with attached PZT source and accelerometer receivers. Extensive corrections for the jacket and the interfaces are however applied in a numerical inversion model to correct for the specimen-rod interface effects. Table 3 lists authors and techniques that have successfully probed the sonic frequency range as functions of frequency and specimen dimensions categorized into measured parameters. Featured is not only RB and FO but also the Pulse-Tube (PTU), Gas Hydrate Resonant Column (GHRC), and Resonant Ultrasound Spectroscopy (RUS) techniques.

3.2 PULSE-TRANSMISSION (PT)

Pulse-Transmission (PT) was extended from metals [56] to rocks [57–59] and further disseminated [60–62] as a technique. PT determines the travel-time of an elastic wave propagating between two PZC (normally quartz or PZT) transducer elements in which one generates and the other records the ultrasonic pulse. The piezoceramic size determines its resonant (or center) frequency. Scattering effects are avoided if specimen heterogeneities are eclipsed in size by the wavelength. Since distance travelled (equals specimen length) and travel-time are known, the basic equation of motion yields velocity based on the time of flight principle. Piezoceramic (PZC) elements deform mechanically and generate electricity respectively as external voltages and forces are applied. P- and S-wave transducers are sensitive to their respective wave types.

Polarization-alignment is paramount for the S-wave transducers due to the physical nature of S-waves. In practice, the quality of the signal depends on the transducer-specimen coupling being adequate or inadequate while the accuracy of the measurements is related to the adequacy of the velocity picks. Normal P-waves are trivial but oblique P-waves and any S-waves are non-trivial to pick. Practice and theory are advanced by transducer and algorithm novelty. Eternal is the group versus phase velocity conundrum for oblique P-waves that depend on transducer size. PT attenuation is determined by the Spectral Ratio (SR) method which compares spectral amplitudes at different distances from the slope of the logarithmic decrement [15]. Otherwise attenuation is also determined by comparing two geometrical identical specimens: a non-dispersive reference specimen and the studied specimen [8]. This is the same principle as for FO in comparing non-dispersive reference specimens with dispersive rock specimens. Pulse-Echo (PE) is physically different from PT (echo versus transmission) but principally similar in determining attenuation by standard-specimen comparisons.

3.3 FORCED-OSCILLATION (FO)

Bruckshaw and Mahanta [63], Peselnick and Outerbridge [64], and Usher [65] performed the first Forced-Oscillation (FO) measurements that determined the intrinsic attenuation and elastic moduli of rocks. The two extremes investigated the longitudinal mode (Young’s modulus E and attenuation Q_E^{-1}), whereas the middle developed a pendulum able to generate harmonic torques (shear modulus G and attenuation Q_G^{-1}). Truth be told, Norton [66] and Kê and Ross [67] measured the internal friction of metals using torsional pendulums before Peselnick and Outerbridge [64] extended it to rocks. As did Koppelman [68] who described several flexural and torsional pendulum and wave propagation devices for the study of polymers. Strain amplitude was not controlled in the first generation of FO experiments but was later constrained to 10^{-6} to remain within the linear elastic domain [69]. Spencer [21] measured the stress-strain behaviour of rocks via transducers recording the axially applied sinusoidal force and the resulting displacement. Adelinet et al. [70] applied hydrostatic oscillations to measure bulk modulus K of isotropic rocks via confining pressure pulsations. Jackson et al. [71] modified their torsional capabilities to also accommodate for measurements of the flexural mode which Woïrgard et al. [72] and Woïrgard and Guéguen [73] also measured for metals and rocks in the past. Unlike Adelinet et al. [70], Lozovyi and Bauer [74] enforced uniaxial instead of hydrostatic conditions by adding axial oscillations to investigate anisotropic rocks. Suarez-Rivera et al. [75] measured uniaxial modulus decades before Lozovyi and Bauer [74] without disclosing any details about the apparatus. FO requires (i) a force generator with alterable frequency, (ii) a force sensor to estimate the applied stress, and (iii) strain sensors for the specimen. Modulus and attenuation are given by the stress-strain ratio and the phase angle between the stress and the strain (or the area of the hysteresis loop), respectively. If an elastic standard is chosen over a transducer to measure the stress, modulus and attenuation are given by the relative strain amplitude of the standard versus the specimen and the phase angles between the standard and the specimen. Table 4 tabulates apparatuses for (i) longitudinal, (ii) torsional, (iii) flexural, (iv) volumetric, and (v) uniaxial stress-strain oscillations. Type (ii), (iii), and (iv), and (v) apparatuses exist but type (i) is still predominant.

FO is theoretically trivial but practically non-trivial. Misalignments related to manufacturing tolerances primarily affecting attenuation measurements (inconsistent phase angles) are particularly challenging [76–78]. In the case of Rørheim and Holt [6], this problem originated from misaligned interfaces. Uneven stress distribution may be observed on the semiconductor resistivities during axial loading. Numerous approaches have been applied to alleviate systematic errors caused by misalignment if all interfaces are not flawlessly parallel and smooth when

manufactured. Paffenholz and Burkhardt [79], Takei et al. [80], and Ikeda et al. [81] neutralized potential misalignments with three axially symmetrical transducers. Resonances enforce a natural upper limit for FO measurements in the low-frequency regime. Due to the nature of resonances (nodes and antinodes as well as their distribution), Batzle et al. [33] extended this limit by identifying the antinodal frequencies and adjust the measurements accordingly. Fluid-flow related dispersion occurring at the intermediate sonic frequency range may be inferred by using a very viscous fluid as described by Fortin et al. [82] and Pimienta et al. [83]. Since the time-scale of diffusion processes are related to the dynamic viscosity of the fluid, the frequency of the measurement can be scaled by the viscosity of the fluid [84].

Despite being less sensitive to resonances than other transducers, strain gauges are largely limited to investigating pore-scale processes [85]. Averaging multiple strain measurements at different positions on the specimen surface may however approximate the bulk mechanical properties of a rock [86]. The smaller the specimen, the better the averaging result (proportional to the covered area). Chapman and Quintal [85] favoured measuring bulk strain (cantilevers) in addition to or instead of local strains (strain gauges) due to the locality of heterogeneities. Bulk-strain approaches are superior for isotropic rather than anisotropic rocks due to Poisson's ratios being problematic to measure. Tisato [87] explained the double-interface problem related to radial cantilevers on jacketed (sealed) specimens. Spencer [21] however solved this problem with non-contact capacitive sensors and Tisato [87] explored [88] effect sensors. Fibre optic DAS is another possibility [86, 89–91] that faces similar problems. Simultaneous bulk and local strain measurements could perhaps also distinguish between microscopic and mesoscopic dispersion and attenuation mechanisms [85]. Unlike Adam and Batzle [92] but like Chapman and Quintal [85], Sun et al. [93] analyzed individual strains before averaging to distinguish local from global flow. Stress-strain signal magnitudes and phases are computed by FFT after being digitized and averaged by physical or virtual lock-in amplifiers.

FO is applied to measure properties of all sedimentary rock types: sandstones [21, 33, 43, 79, 89, 90, 93–135], carbonates [21, 33, 64, 79, 92, 99, 100, 119, 120, 136–149], and shales [75, 100, 119, 150–160]. FO is also applied to igneous rocks [21, 70, 71, 73, 161–164] that are beyond the scope of this study (due to their non-sedimentary nature) but are nonetheless represented in Table 4. Suarez-Rivera et al. [75] is the only inter-frequency study comparing FO, RB, and PT. McCann et al. [165] used FO to measure fluid properties (bulk modulus K and attenuation Q_K^{-1}) at high pressures. Be advised that Table 4 may list the same apparatus multiple times because they are continuously being improved or adjusted with time. Subramaniyan et al. [7] summarized attenuation studies on conventional reservoir rocks (i.e. sandstones and carbonates), while we added studies of recent conventional rocks as well as unconventional shales to update and complete the list:

Sandstones Spencer [21] initially observed negligible Q_E^{-1} of a vacuum-dried Navajo specimen that eventually became significant once saturated with water, ethanol, or n-decane. Paffenholz and Burkhardt [79] evaluated four different sandstones at different saturation levels and observed that E and G decrease with increasing saturation at $< 50\%$ saturation but is independent of water content at $> 50\%$ saturation. In comparison, Q_E^{-1} and Q_G^{-1} are less pronounced with decreasing saturation and their peaks shift towards higher frequencies. Yin et al. [95] studied Berea specimens using FO and RB: Q_E^{-1} increases with frequency and brine-saturation. Cherry et al. [96] saw E stiffening and Q_E^{-1} weakening of a Lyon's specimen with decreasing saturation. Chelidze et al. [97] also studied Lyon specimens but instead the effect of acetone and water-surfactant on E and Q_E^{-1} . Q_E^{-1} of dry or fluid-saturated ($< 50\%$) Berea specimens are low and approximately frequency-independent [94, 101, 102, 104, 106, 111, 166] or high and frequency-

dependent [102, 104, 105, 108, 109, 111, 167]. Batzle et al. [33] attributed such behaviour to fluid mobility M_F defined as $M_F = k/\eta$ where k is permeability and η is viscosity without presenting Q_E^{-1} of actual rocks: deflating M is coupled with inflated relaxation time required to equilibrate the pore pressure. Fluid-saturated rocks will consequently appear stiffer under conditions in which the period of elastic perturbation is shorter than the fluid relaxation time than at lower frequencies. David [103] attempted to measure E , Q_E^{-1} , and ν of dry, water and glycerine-saturated Fontainebleau specimens but ultimately questioned the reliability of the results due to inconsistencies related to FO eclipsing PT in E and ν magnitudes. Tisato and Quintal [106] explained their high and frequency-dependent Q_E measurements for a nearly fully water-saturated Berea specimen by WIFF at the mesoscopic scale. Mikhaltsevitch et al. [109] observed decreasing and frequency-dependent Q_E^{-1} with increasing confining pressure culminating at 1 Hz for a fully water-saturated Donnybrook specimen. Spencer [107] measured E and Q_E^{-1} as well as ν and Q_ν^{-1} in McMurray bitumen sand specimens containing residual air where calculated Q_P^{-1} , Q_K^{-1} , and Q_G^{-1} peaks shifted towards lower frequencies as viscosity increased (by decreasing temperature) demonstrating strongly viscosity-dependent attenuation mechanisms.

Tisato et al. [29] provided the first experimental evidence of WIGED in gas (air, N_2 , or CO_2) and water equilibrated Berea specimens which was also numerically supported. Subramaniyan et al. [168] disclosed that “a decrease in viscosity of the saturating fluid shifted the attenuation curve to higher frequencies” while “an increase in confining pressure caused a decrease in the overall magnitude of attenuation” in Fontainebleau specimens. “Squirt-flow” is implied as the dominant mechanism for their glycerine data. Pimienta et al. [169, 170] studied E and K frequency dependence and attenuation in water and glycerine-saturated Fontainebleau specimens. Two frequency-dependent phenomena interpreted as drained-undrained and undrained-unrelaxed E -transitions [169] and underestimation of the drained-undrained transition implying a direct drained-unrelaxed K -transition [170] are observed. Spencer and Shine [110] concluded that “the modulus dispersion and attenuations (Q_P^{-1} and Q_G^{-1}) in saturated sandstones are caused by a pore-scale, local-flow mechanism operating near grain contacts.” Chapman et al. [111] measured E and Q_E^{-1} of a Berea specimen at various saturation levels and confining pressure: attenuation negligible at $< 80\%$ and significant at $> 91\%$ saturation also reduced and shifted towards lower frequencies by increasing confining pressure. Consistent with WIFF in response to heterogeneous water distribution in the pore space (patchy saturation), high enough fluid pressure to ensure full saturation also renders attenuation negligible. Ma et al. [112] attempted to validate their apparatus by aluminum and lucite measurements: E and ν but no Q_E^{-1} . V_P and V_S converted from E and ν also increased with pressure and saturation. Mikhaltsevitch et al. [43] demonstrated the causality-consistency of dry and water-saturated Donnybrook and Harvey as well as glycerol-saturated Berea specimens using KKR. Tisato et al. [113] proved the feasibility of combining FO with μ CT [171] to study a dry and partially saturated Berea specimen from 0.1 to 25 Hz in a CT-transparent cell. Insignificant changes between these different conditions aside, this was the first time elastic measurements and imaging was combined for FO. Explained by a transition from WIFF to WIGED and inspired by Tisato et al. [29], Chapman et al. [172] observed a significant steepening of the high-frequency asymptote of the measured

attenuation in Berea specimens caused by a minor change in water saturation (but a significant modification in the pore fluid distribution). Pimienta et al. [114] reported drained-undrained transitions in Wilkenson, Berea, and Bentheim specimens saturated by fluids of varying viscosities. Berea features E and ν dispersion as well as Q_E^{-1} and Q_ν^{-1} attenuation towards higher frequencies. Bentheim and Wilkenson only feature E dispersion and Q_E^{-1} attenuation. Pimienta et al. [114] interpreted Wilkenson’s consistency and Bentheim’s inconsistency with Zener’s model [35] as “squirt-flow” or measurement inaccuracy (possibly also another physical effect). Sun et al. [115] measured two attenuation peaks probably caused by two different mechanisms for a tight sandstone saturated between 45 and 85% but no peaks beyond these limits.

Sun et al. [116] focused on presenting an enhanced FO version void of subsonic resonances based on numerical modelling but also included inconclusive E and ν measurements. Chapman et al. [117] observed “frequency-dependent attenuation and the associated moduli dispersion in response to the drained–undrained transition (0.1 Hz) and ‘squirt-flow’ (> 3 Hz)” in Berea specimens. Yin et al. [118] sought to elucidate Gassmann’s fluid substitution theory by studying a clay-bearing Thüringen specimen by combining FO and PT. Dry specimens are non-dispersive (and thus non-attenuative) whereas water-saturated specimens are dispersive (and thus attenuative) which is attributed to the drained-undrained transition. Gassmann’s theory is consistent with their undrained K but not with their water-softened G which is significant at seismic but masked by “squirt-flow” stiffening at ultrasonic frequencies. Yin et al. [118] ascribed this reduction in surface free energy to chemical interaction between pore fluid and rock frame which eludes Gassmann’s theory. Li et al. [120] observed a broad distribution of E and Q_E^{-1} across 1-1000 Hz with peak attenuation at 60% saturation in a tight sandstone. Borgomano et al. [121] enforced drained or undrained conditions on glycerine-saturated or -unsaturated Bleurswiller specimens for K and Q_K^{-1} determination with microvalves (combined dead volume less than 40 μ l). Gallagher et al. [122] focused on dry, brine-, and glycerine-saturated sandstones. Sun et al. [123] compacted Bleurswiller specimens beyond “the critical pressure which characterizes the onset of pore collapse and grain crushing” to the point that the critical frequency of “squirt-flow” dispersion (relaxed-unrelaxed transition) was shifted towards higher frequencies beyond the seismic band “allowing Biot-Gassmann to fully apply”. This result was interpreted as a consequence of increased crack aspect ratio after compaction. Li et al. [124] complimented the tight rocks of Li et al. [120] with a weakly consolidated sandstone. Also a study about saturation effects, peak attenuation occurs at 60 Hz and at 79% saturation. Ògúnsàmi et al. [125] performed the first systematic inter-laboratory study applying three different FO devices to cross-validate the elastic properties of a reservoir sandstone. Inter-laboratory frequency and fluid-saturation effects are consistently proven pressure-dependent at dry and decane-saturated conditions. Sun et al. [93] investigated the impact of microstructure heterogeneity and local measurements on dispersion and attenuation of dry plus brine- and oil-saturated Shahejie specimens from 1 to 300 Hz. Local diverges from global flow by being influenced by the position of the strain gauges which Sun et al. [93] attributed to crack-aspect-ratio heterogeneity since porosity and crack density are homogeneous. Sun et al. [93] measured not only E and Q_E^{-1} but also ν and Q_ν^{-1} owing to biaxial semiconductor strain gauges.

Zhao et al. [126] discovered one or two attenuation peaks related to micro- and mesoscopic flow between 1 and 2000 Hz affected by saturation degree, oil viscosity, and confining pressure. A dual-scale fluid flow model suggested “that the attenuation mechanisms at different scales interplay with each other and jointly dominate the attenuation behavior of the partially saturated specimen.” Yurikov et al. [89, 90] explored fibre optic DAS instead of strain gauges on a dry Bentheimer specimen. Chapman et al. [127] observed significant E and K but insignificant G dispersion and attenuation caused by fluid pressure diffusion (FPD) in partially saturated Berea specimens featuring CO₂-exsolution by depressurisation. Tisato et al. [128] measured dry and partially saturated Berea specimens as function of confining pressure in which the former are frequency-independent and the latter are frequency-dependent at pressures below 14 MPa. Tisato et al. [128] also used KKR-consistent models to determine the mechanism WIFF but was unable to distinguish between “squirt-flow” and patchy-saturation as sub-mechanisms. Wei et al. [173] assumed isotropy to convert K and Q_K^{-1} from measured E and Q_E^{-1} plus ν and Q_V^{-1} for two sandstones at different saturation states. Bentheimer and Bandera are opposites: K dispersion is entirely absent in the former but present and increasing with saturation in the latter. Peculiar is however that only converted and no measured parameters are disclosed. Han et al. [129] measured significant Young’s modulus E and Poisson’s ratio ν transformed to P- and S-wave velocities V_P and V_S dispersion at seismic and insignificant dispersion from seismic to ultrasonic frequencies for oil- and glycerine-saturated tight sandstones. He et al. [130] extended on previous studies by introducing a squirt-flow extended patchy saturation model: V_P is both measured and modelled but $Q_{V_P}^{-1}$ is only modelled. Ma [131] studied V_P of water- and glycerine-saturated specimens. Riabokon et al. [132] studied the non-linearity of 286 dry specimens at different strain amplitudes where Eddy Current Probe (ECP) and Laser Vibrometer (LV) measured axial and radial strains. Lu [133] measured axial and shear strains of artificial specimens (3D printed and otherwise) at different stress and loading conditions from 0.01 to 20 Hz using a pair of Laser Displacement Sensors (LDS). Chapman et al. [134] questioned the assumed adiabatic (thermodynamically unrelaxed) and instead argued for isothermal (thermodynamically relaxed) interaction between multiple fluid phases by studying microscopic gas bubbles. Evident E , K , and G dispersion and Q_E^{-1} , Q_K^{-1} , and Q_G^{-1} attenuation peaks at ~ 100 Hz are interpreted as thermodynamic relaxed-unrelaxed transitions. G and Q_G^{-1} are possibly affected by pore-scale heterogeneities as experiments and numerics coincide. Yurikov et al. [91] is a reiteration of Yurikov et al. [89, 90]. He et al. [135] combined FO and PT to calculate and measure V_P for three dry, brine-, and glycerine-saturated sandstones as a function of effective pressure. Pore microstructure significance is implied by simultaneously increasing effective pressure and decreasing dispersion as well as simulated by a triple porosity model with combined “squirt-flow” effects. Triple signifies equant, intermediate, and compliant pores with inhomogeneous aspect ratio distributions.

Carbonates Spencer [21] measured E and Q_E^{-1} of Spargen specimens at different saturation and temperature conditions. Spencer’s vacuum-dried specimen is the stiffest and least dispersive and attenuative but his water-saturated specimens are increasingly attenuative and dispersive yet softer from 2°C to 25°C. Paffenholz and Burkhardt [79] also observed E and G stiffening with corresponding Q_E^{-1} and Q_G^{-1} weakening as a function of decreasing saturation. Batzle et al. [33] studied

P- and S-wave velocities as a function of frequency and temperature for heavy oil-saturated Uvalde specimens that decreased in velocities with increasing temperature. Adam et al. [136] explored Gassmann’s theory applicability to G and K dispersion in what was claimed the first controlled laboratory experiments on carbonates at seismic frequencies. Behura et al. [137] saw significant Q_G^{-1} temperature dependence (and thus viscosity dependence) in bitumen-saturated Uvalde specimens similar to the observations of Spencer [107] for McMurray bitumen sand. Adam et al. [138] calculated Q_K^{-1} , Q_P^{-1} , and Q_G^{-1} from measured Q_E^{-1} and the complex ν . In contrast to sandstone observations, Q_E^{-1} is higher when dry rather than fully water-saturated: Q_E^{-1} is frequency-dependent in both dry and saturated scenarios. Zhao et al. [139, 140] are the same study presented twice: FO, DARS, and PT are combined to measure V_P and V_S in partially saturated specimens across seismic, sonic, and ultrasonic frequencies. Mikhaltsevitch et al. [141] also studied Gassmann’s theory applicability for elastic moduli prediction and the influence of partial water saturation on elastic and anelastic properties of Savoinnière specimens. Borgomano et al. [142] found dispersion at around 200 Hz affecting all moduli but G in water-saturated Lavoux specimens. Mikhaltsevitch et al. [143, 144, 147] demonstrated that non-ideal boundary conditions (enforced by varying dead volumes) caused significant dispersion in fully decane-saturated Savoinnière specimens if the dead volume exceeds the pore space. Borgomano et al. [145] interpreted the observed dispersion and attenuation of Coquina, Rustrel, and Indiana (intact and thermally cracked) specimens in terms of transitions between drained, undrained and unrelaxed fluid-flow regimes at water and glycerine-saturated conditions. Biot-Gassmann theory consistency is proven at seismic frequencies. Pore type is correlated to “squirt-flow” dispersion absent in rocks featuring intragranular microporosity and present in rocks featuring cracked intergranular cement and uncemented grain contacts at seismic and sonic frequencies. Li et al. [120] also studied a tight carbonate at various degrees of saturation devoid of any noteworthy attenuation and dispersion features beyond an accretion of Q_E^{-1} towards 1000 Hz. Tan et al. [174] complemented Mikhaltsevitch et al. [144] with a 1D poroelastic model based on Müller and Sahay [175] that quantified the dead volume dependence predicted by Pimienta et al. [83] and Sun et al. [176]. Ikeda et al. [177] measured increasing E and decreasing Q_E^{-1} with increasing water-saturation for a polymineralic carbonate. Riabokon et al. [146] also studied the non-linearity of dry carbonates. Mikhaltsevitch et al. [147] is the continuation of Mikhaltsevitch et al. [143, 144] whose results are also modelled by modified Gassmann theory. Sun et al. [148] studied the impact of partial saturation by (i) drying and (ii) imbibition: P-wave dispersion (and attenuation) is significant for (i) but not for (ii) whereas S-wave dispersion (and attenuation) is insignificant for both (i) and (ii) at $> 80\%$ RH. Mesoscopic WIFF controlled by geometry and pore fluid distribution is the main mechanism causing P-wave dispersion. Gallagher et al. [149] hydrostatically investigated unfractured and fractured Rustrel specimens [145] at different effective pressures in triaxial and undrained conditions to better understand the effect of fractures and validate computational fracture models. Aside from a local negative phase shift for the fractured specimen at saturated conditions, no attenuation is observed at dry conditions.

Shales

Duranti et al. [150] discovered that dispersion in shales occurs between sonic and ultrasonic frequencies in addition to the seismic band being characterized by

nearly constant attenuation. Hofmann [100] and Sarker and Batzle [151] studied the frequency dependence of water and glycerine saturated Mancos specimens. Despite proven able to measure Q_E^{-1} [33], Hofmann [100] and Sarker and Batzle [151] solely focused on E and ν converted into V_{P_0} , $V_{P_{45}}$, $V_{P_{90}}$, V_{S_0} , and $V_{S_{90}}$ via C_{ij} . Delle Piane et al. [152, 153] made a two-fold discovery: (i) attenuation is greater normal to bedding, and (ii) partial saturation increases the attenuation (likely due to micro and mesoscopic flow). Failure to disclose E and ν was due to deficient calibration of the absolute displacement signals related to different amplification factors. Mikhaltsevitch et al. [154] linked seismic and ultrasonic measurements of dry and wet 0° Eagle Ford specimens found to be non-dispersive and non-attenuative by assuming isotropy. Both measurement types were concluded to be in the high-frequency regime due to partial saturation. Huang et al. [155] measured Mancos dispersion and attenuation: $E_V > E_H$ and $Q_{E_V}^{-1} > Q_{E_H}^{-1}$. Low Q_E was also measured for Xianjing specimens. Mikhaltsevitch [157] studied dispersion and attenuation of fully saturated Wellington (0, 45, and 90°) and a partially saturated Mancos (0 and 90°) specimens. $Q_{E_{45}}^{-1} > Q_{E_H}^{-1} > Q_{E_V}^{-1}$ appears to be a clandestine trend within the scattered Wellington data $Q_{E_x}^{-1} < 0.0075$ in which x refers to subscripts V , H , and 45 . Trend or no trend, Mikhaltsevitch [157] measured Wellington at non-dispersive frequencies due to the low $Q_{E_x}^{-1}$ devoid of any noteworthy peaks. Like Wellington $Q_{E_V}^{-1}$ and $Q_{E_H}^{-1}$, Mancos $Q_{E_V}^{-1}$ and $Q_{E_H}^{-1}$ are also insignificant and unnoteworthy at RHs below 97.5%. Unlike at other RHs, 97.5% features $Q_{E_V}^{-1}$ and $Q_{E_H}^{-1}$ peaks. $Q_{E_V}^{-1} > Q_{E_H}^{-1}$ and $E_H < E_V$ universally applies to Mikhaltsevitch [157] who also observed gradual softening accompanied by monotonically decreasing E_V and E_H with increasing saturation. Mikhaltsevitch et al. [178, 179] are based on the Wellington experiments summarized in Mikhaltsevitch [157]. Mikhaltsevitch et al. [180] is the recent extension of the Mancos experiments [157, 181, 182]. Anisotropic permeability is their explanation to peak $Q_{E_V}^{-1}$ and $Q_{E_H}^{-1}$ occurring at different frequencies. Global flow ensured by the drained-undrained transition explains the presence or absence of dispersion at the probed frequencies. Wellington is also studied by Mikhaltsevitch et al. [160] but at different saturation states with similar dispersion features (and explanation) as Mancos [180]: peak $Q_{E_V}^{-1}$ and $Q_{E_H}^{-1}$ at 2 and 6 Hz. Mikhaltsevitch et al. [160] also includes the Eagle Ford experiments by Chavez et al. [119]. Rørheim [4] observed non-simultaneous uniaxial-stress E_V and uniaxial-strain C_{33} behaviours as well as decreasing $Q_{E_V}^{-1}$ and $Q_{C_{33}}^{-1}$ with decreasing saturation for five differently oriented and saturated Pierre specimens. E_V is doubled once and ν_{VH} is halved twice with decreasing saturation. $E_V < E_{45} < E_H$ is continuous while initially $Q_{E_H}^{-1} < Q_{E_{45}}^{-1} < Q_{E_V}^{-1}$ ultimately becomes $Q_{E_V}^{-1} < Q_{E_H}^{-1} < Q_{E_{45}}^{-1}$ with increasing frequency. FO-measured C_{33} and PT-measured V_{P_0} decrease simultaneously with decreasing saturation despite the frequency gap. No $Q_{E_V}^{-1}$ attenuation peaks but E_V dispersion were noticed.

Although unable to record Q_E^{-1} measurements, Szewczyk et al. [183] observed strong softening at seismic and hardening counteracting this softening at ultrasonic frequencies (due to increasing dispersion) with increasing water saturation in Mancos specimens. ν also strongly increased but appeared nearly frequency-independent. Types of shales also differ in stress sensitivity during hydrostatic loading which also differs at seismic and ultrasonic frequencies. Li et al. [158] referred to Huang et al. [155] when measuring E and ν dispersion of an un-

named field shale. Szewczyk et al. [184] assumed variable and linearly decreasing C_{ij}^{dry} with increasing RH for anisotropic Gassmann’s theory to be applicable to Mancos. Lozovyi [159] succeeded Szewczyk [185] by comparing the static and dynamic stiffness of Opalinus Clay and three other anonymous specimens [186–188]. Chavez et al. [119] conducted FO creep tests on three dry sedimentary rocks at constant 2 Hz for 120 hours. Creep effects significantly impacted the moduli for all three specimens but the shale was most affected. Mikhaltsevitch et al. [180] questioned the applicability of anisotropic Gassmann theory to Mancos proposed by Szewczyk et al. [184] on the basis that $C_{ij}^{\text{sat}} > C_{ij}^{\text{dry}}$ is repudiated by the non-linearity of the decreasing C_{44} and C_{66} with saturation. Be the fact that $C_{44}^{\text{sat}} < C_{44}^{\text{dry}}$ and $C_{66}^{\text{sat}} < C_{66}^{\text{dry}}$ as it may, the non-linearity is questioned (only applies to C_{44} and C_{66} at 9% RH). Rørheim et al. [189] performed FO measurements as functions of frequency as well as time on a CO₂-exposed Draupne specimen where E_V and ν_{VH} insignificantly changed over 575 hours. Neither PT measured V_{P_0} nor V_{S_0} significantly changed perhaps due to Draupne’s low calcite content. Rørheim et al. [190] combined FO and PT at elevated temperatures for 0 and 90° Pierre specimens: FO measured E_V and E_H dispersion shifted towards higher frequencies while FO converted and PT measured V_{P_0} , $V_{P_{90}}$, V_{S_0} , and $V_{S_{90}}$ oppositely decreased and increased with temperature. Two simple frequency-dependent bound water models were also proposed.

Numerical studies supplementing experimental ones are becoming customary. Experimentally proven by Tisato and Madonna [102], Quintal et al. [191] and Quintal et al. [192] were the numerical impetus of Chapman and Quintal [85], Tisato and Quintal [106], Chapman et al. [127, 134], Gallagher et al. [149], Tisato and Quintal [166], Kuteynikova et al. [167], Quintal et al. [193], Hunziker et al. [194], Quintal et al. [195], Alkhimenkov et al. [196], Lissa et al. [197–200], and Alkhimenkov and Quintal [201, 202] in terms of attenuation modelling. Zhang and Toksöz [203], Das et al. [204], and Jänicke et al. [205] used similar Digital Rock Physics (DRP) approaches to study attenuation mechanisms and fluid-solid interactions. Balcewicz et al. [206] used DRP to study other properties. Focusing on enhancing an existing FO approach, Sun et al. [116] tried to alleviate the experimental destructive subsonic resonances via numerical modelling to redefine their apparatus design. Sun et al. [116] achieved this by inverting Tittmann’s principle manifested by Nakagawa’s loaded resonator: the shorter the apparatus, the higher the characteristic frequency. Sun et al. [116] inspired Liu et al. [207] to investigate the cause and effect of subsonic resonances for the apparatus described by Mikhaltsevitch et al. [109] in a similar manner. Sun et al. [176] 3-D modelled the drained-undrained transition for the frequency-dependent elastic moduli and attenuation. In order to inaugurate an upper frequency-limit, Borgomano et al. [121] and Li et al. [208] adopted the COMSOL-based numerical approach by Sun et al. [116] to deduce at which frequencies their apparatus resonates. Unlike Sun et al. [116] and Borgomano et al. [121], Li et al. [208] included jointing conditions in their model because the stress-field is non-homogeneous. As a result, elastic properties depend on strain gauge position. Be aware however that numerical need not equal experimental due to the ideal versus non-ideal states predicament. Ikeda et al. [177] compared experimental and numerical results: 10% separates DRP-derived and FO-measured E .

FO implementations are proven by their ability to measure attenuation of standard materials often used for calibration purposes: lucite, aluminum, and PEEK. Other calibration materials exist (e.g. Borgomano et al. [121] calibrated for glass and gypsum in addition to lucite, while Brunner et al. [209] used a unspecified “viscoelastic structure”) but are excluded due to their rarity. To the best of their knowledge, Rørheim and Holt [6] compiled and studied all

published FO measurements involving these three materials (Table 2) to validate their findings by literature comparison (Figure 6³). Lucite is dispersive opposed to non-dispersive aluminum and PEEK. Questioned is the calibration applicability of high modulus aluminum dissimilar to rocks but not that of low moduli lucite and PEEK similar to rocks. Batzle et al. [33] recognized that the composition of lucite can be variable from batch to batch. In fact, Bonner [210] claimed that the hardener-resin ratio determines the quality of the material. Unlike the inexpensive resin, the hardener is expensive. It is thus common for resin to be the dominant component of the hardener-resin ratio. This primarily affects the absolute mechanical properties but not the overall frequency dispersion characteristics [164]. Figure 6 possibly features this effect as Sun et al. [116] is an evident outlier compared to all others.

Table 2 All known Q_E measurements of lucite, aluminum, and PEEK alphabetically sorted and categorized by author(s) and specimen material, respectively. Color-bars based on Author # and the (cividis) color-map are used instead of legends. **Rørheim and Holt [6]** is in bold because this is based on that study in which all known FO studies were compared.

Author(s)	Author #	Specimen(s)		
		Lucite	Aluminum	PEEK
Batzle et al. [33]	1	✓	✗	✗
Borgomano et al. [121]	2	✓	✗	✗
Cherry et al. [96]	3	✗	✓	✗
Flidner and French [211]	4	✓	✓	✗
Huang et al. [155]	5	✓	✗	✓
Katzmann et al. [212]	6	✓	✗	✗
Koppelman [68] via Lakes [213]	7	✓	✗	✗
Li et al. [158]	8	✗	✓	✗
Lienert and Manghnani [94]	9	✓	✗	✗
Liu and Peselnick [77]	10	✓	✗	✗
Lu [133]	11	✓	✓	✗
Madonna et al. [214]	12	✓	✓	✗
Madonna and Tisato [104]	13	✓	✓	✗
McCann [215]	14	✓	✓	✗
Mikhaltsevitch et al. [141]	15	✓	✗	✗
Nakagawa [105]	16	✓	✗	✗
Paffenholz and Burkhardt [79]	17	✗	✓	✗
Pimienta et al. [169]	18	✓	✗	✗
Rørheim and Holt [6]	19	✓	✓	✓
Spencer [21]	20	✓	✓	✗
Sun et al. [116]	21	✓	✗	✗
Takei et al. [80]	22	✓	✓	✗
Tisato and Madonna [102]	23	✓	✓	✗
Tisato et al. [113]	24	✓	✗	✗
Yao [216]	25	✓	✓	✗
Yee and Takemori [217]	26	✓	✗	✗
Yin et al. [218]	27	✓	✓	✗

³Please be advised that all external measurements from other authors are digitized with variable resolution during which resonance-affected data are omitted.

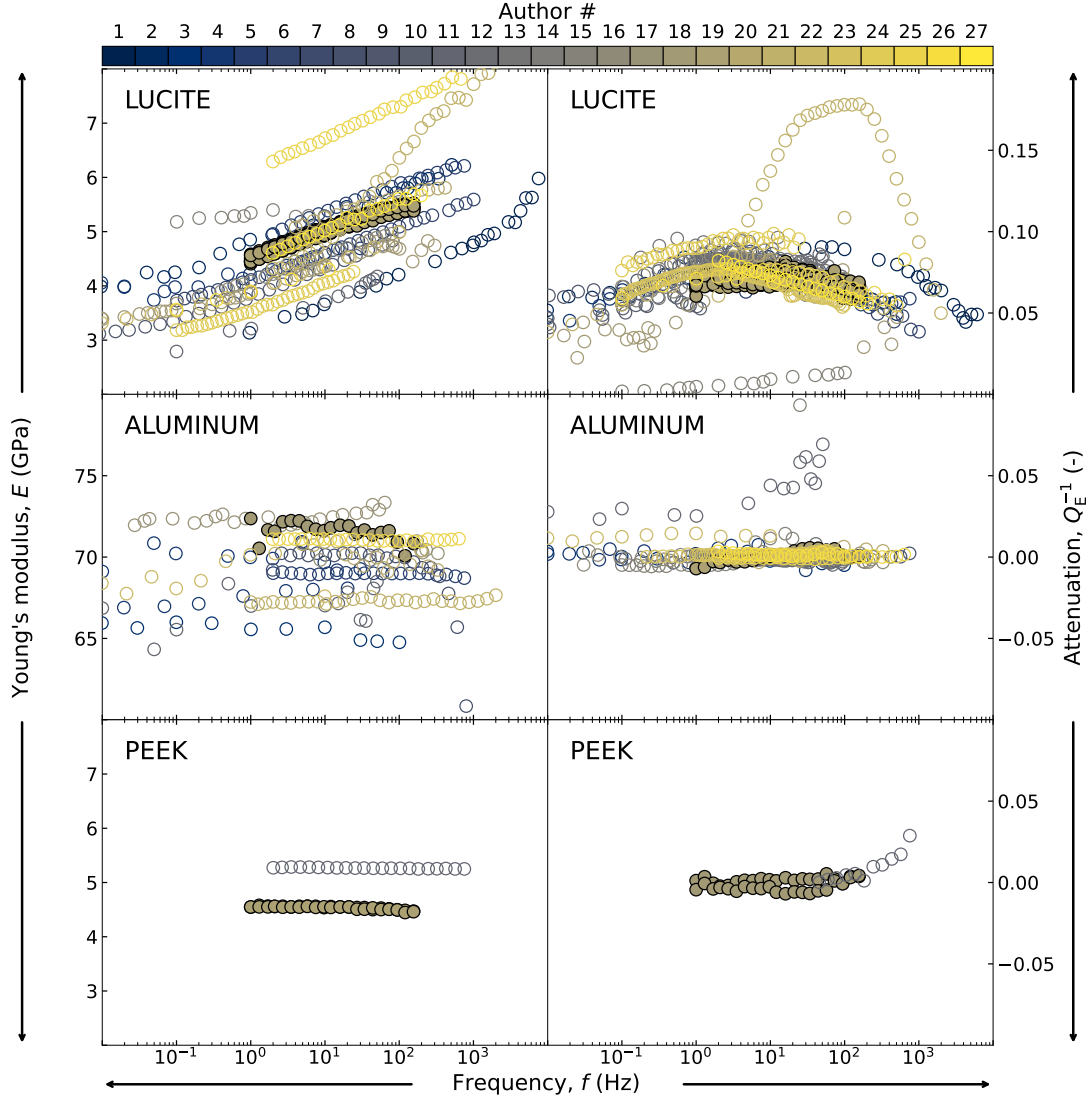


Figure 6 Young’s modulus E and attenuation Q_E^{-1} versus frequency f . Color-bars denote authors according to Author # listed in Table 2. Enhanced distinguishability is ensured by solid symbols for the bolded **Rørheim and Holt [6]** and open symbols for all other authors.

3.4 OTHERS

Beyond the traditional RB, PT, and FO techniques, Resonant Ultrasound Spectroscopy (RUS), Differential Acoustic Resonance Spectroscopy (DARS), and Laser UltraSonics (LUS) are other novel techniques exploited in rock physical research. Maynard [245] not only introduced the term RUS “to encompass all techniques in which ultrasonic resonance frequencies are used to determine elastic moduli” but also traced the history of RUS back to Fraser and LeCraw [246], Schreiber and Anderson [247], and Demarest [248]. In fact, RUS is in many aspects a continuation of RB but differs due to its ability to capture numerous resonance peaks across

Table 3 Sonic frequency probing techniques with primary focus on Resonant Bar (RB) but secondary also on Pulse-Tube (PTU), Gas Hydrate Resonant Column (GHRC), Resonant Ultrasound Spectroscopy (RUS), and Differential Acoustic Resonance Spectroscopy (DARS).

Author(s)	Technique(s)	Frequency (Hz)	Length (cm)	Diameter (cm)	Parameter(s)
Batzle et al. [33]	FO	5 E0 – 2.5 E3			E, V_P, V_S, Q_E
Birch and Bancroft [18]	RB	1.4E2 – 4.5 E3	244	23	Q
Born [48]	RB	9.3E2 – 1.28E4	14 – 124	12	$\delta = \pi Q^{-1}$
Bourbié and Zinszner [8]	RB	3 E3 – 5 E3			V_E, Q
Cadoret et al. [219]	RB	1 E3	110	8	V_E, V_S, V_P
Cadoret et al. [220]	RB	1 E3	110	8	Q_G, Q_E
Gardner et al. [221]	RB	2 E3 – 3 E3	5 – 30.0	5	δ_E, δ_S
Goldberg and Zinszner [222]	RB	5 E3 – 25 E3	25	2.5	Q_P
Ide [44]	RB	4 E3 – 12 E3	25	5.1	E
Harris et al. [223]	DARS	1 E3 – 2 E3			K, Q_K
Jones and Nur [50]	RB	1.7E2 – 3.4 E3			V_S, Q_G
Lucet et al. [224]	RB	5 E3 – 2 E4	25 – 30	2.5	V_E, V_P, Q_E, Q_G
Lucet and Zinszner [225]	RB	3 E3 – 1 E4	30	2.5	Q_E
Lucet and Zinszner [226]	RB	2 E3 – 2 E4			$Q_E, V_S/V_{US}, V_{PP}/V_{PFB}$
McCann et al. [227]	PTU	1 E3 – 1 E4	60	6.9	V_P, Q_P, T
Murphy [228]	RB	3 E2 – 1.4 E4	20 – 100		V_S, V_E, Q_E, Q_G
Murphy [229]	RB	5 E3	20 – 25	19	V_S, V_E, Q_E, Q_G
Nakagawa and Kneafsey [230]	SHRB	3.5E2 – 2.35E3	6.2	3.75	E, G, ν, V_P, V_S, Q
Nakagawa [53]	SHRB	4 E2 – 2.3 E3	6.22	3.81	E, G, ν, V_P, V_S, Q
Nakagawa and Kneafsey [231]	SHRB	3 E2 – 1.5 E3	7.62	3.75	E, G, ν, V_P, V_S, Q
O'Hara [232]	RB	3 E2 – 3 E3	38	2.22	V_E, V_S, δ
Priest et al. [233]	GHRC	4 E2	14	7	Q_E, Q_G
Tittmann [52]	RB	2.2E4 – 2.3 E4			Q_E, Q_G
Tittmann et al. [234]	RB	7 E3 – 9 E3	12	1.5	Q_E
Waite et al. [235]	SHRB	3.6E2 – 1.6 E3	7.62	3.81	V_P, V_S
Wegel and Walther [236]	RB	1 E2 – 1 E5	30	1	Q_E, Q_G
Winkler and Nur [23]	RB	5 E2 – 1.7 E3	100		$V_E, V_S, V_P, Q_E, Q_K, Q_P$
Winkler and Nur [51]	RB	5 E2 – 9 E3	100		$V_E, V_S, V_P, Q_E, Q_G, Q_K, Q_P$
Wyllie et al. [237]	RB	2 E4		1.9 – 2.50	$V_E, V_S, \nu, \delta_E, \delta_S$
Yin et al. [95]	RB	1.6E2 – 1.8 E3	39 – 53	5	E, Q_E
Zadler et al. [238]	RUS	1.4E2 – 8.8 E4	7.1	2.5	Q_E, Q_G, V_P, V_S

Table 4 Comparison of FO apparatuses based on longitudinal, torsional, volumetric, and uniaxial modes. Partly based on Subramanian et al. [7] but improved and updated as the technique became increasingly acknowledged. Institutions are acronymised due to space limitations.

Mode	Author(s)	Specimen(s)	Force generator	Force sensor	Displacement sensor	Frequency (Hz)	Parameter(s)	Institution(s)
(i) Longitudinal	Adam [86]	Lucite	Shaker	Aluminium STD	Fibre optics	5E0 - 2.5 E3	E , Q_E^{-1} , ν	CSM
	Batzle et al. [33]	Sandstone	Shaker	Aluminium STD	Strain gauge S	5E0 - 2.5 E3	E , Q_E^{-1} , ν	CSM
	Borgomano et al. [121]	Limestone	PZT actuator	Aluminium STD	Strain gauge F	4E-3 - 1 E3	E , Q_E^{-1} , ν	ENS
	Bruckshaw and Mahanta [63]	Various	Coils	Coils	Coils	4E1 - 1.2 E2	E , $\Delta W/W$	ICL
	Cherry et al. [96]	Sandstone	PZT actuator	Aluminium STD	Interferometer	1E-3 - 1 E2	E , Q_E^{-1} , ν	UCB
	Delle Piane et al. [153]	Shale	Motor	Load cell	Strain gauge cantilever	1E-1 - 1 E2	E , Q_E^{-1} , ν	ICL
	David [103]	Sandstone	PZT actuator	Aluminium STD	Strain gauge S	1E-3 - 3 E2	E , Q_E^{-1}	ETH
	Flechner and French [239]	Schist	PZT actuator	Aluminium STD	Strain gauge F	5E-2 - 1.5 E1	E , Q_E^{-1}	RU
	Forth et al. [240]	Sandstone	PZT actuator	Load cell	Strain gauge S	2E0 - 8 E2	E , ν , A , θ	ENS
	Huang et al. [155]	Shale	PZT actuator	Aluminium STD	Strain gauge S	1E-1 - 1 E2	E , Q_E^{-1}	UH
	Ikeda et al. [81]	Lucite	PZT actuators	Titanium STD	Capacitive sensor	1E-2 - 1 E3	E , Q_E^{-1} , ν , Q_v^{-1}	UT(A)
	Katzmann et al. [212]	Sandstone	PZT actuator	Aluminium STD	Strain gauge F	1E-1 - 1 E2	E , Q_E^{-1}	US
	Lienert and Manghnani [94]	Sandstone	Shaker	PZT transducer	Capacitive probe	1E-1 - 1 E2	E , Q_E^{-1}	UoH
	Li et al. [158]	Shale	PZT actuator	Aluminium STD	Strain gauge S	2E0 - 8 E2	E , ν , A , θ	UH
	Li et al. [241]	Sandstone	Shaker	Aluminium STD	Strain gauge	5E0 - 2 E3	E , ν	Sinopec
	Lu [133]	Sandstone	MTS actuator	Load cell	Laser	1E-2 - 5 E1	E	UofA
	Madonna and Tsato [104]	Sandstone	PZT actuator	Aluminium STD	LVDT's	1E-2 - 1 E2	E , Q_E^{-1}	ETH
	Mikhailovitch et al. [109]	Sandstone	PZT actuator	Aluminium STD	Strain gauge S	1E-1 - 4 E2	E , Q_E^{-1} , ν	CU
	Nakagawa [105]	Sandstone	PZT actuator	Load cell	Gauges attached to two rings	1E-3 - 1 E2	E , G , Q_E^{-1} , Q_G^{-1}	LBL
	Paffenholz and Burkhardt [79]	Various	PZT transducer	PZC transducer	Inductive transducer	3E-3 - 3 E2	E , Q_E^{-1}	TUB
	Peschnick et al. [161]	Granite	Capacitive transducer	Capacitive transducer	Capacitive transducer	2E-1	E , Q_E^{-1}	USGS
	Riabokon et al. [132]	Sandstone	PZT actuator	Signal generator	ECF and LV	5E0 - 4 E1	E	UA
	Spencer [21]	Various	Shaker	PZT transducer	Displacement transducer	4E0 - 4 E2	E , Q_E^{-1}	Chevron
	Sun et al. [116]	Sandstone	Shaker	Aluminium STD	Strain gauge S	1E0 - 2 E3	E , Q_E^{-1} , ν	CUP
	Sun et al. [93]	Sandstone	PZT actuator	Aluminium STD	Strain gauge F	1E0 - 3 E2	E , Q_E^{-1} , ν , Q_v^{-1}	ENS
	Szewczyk et al. [183]	Shales	PZT actuator	PZT (Kistler)	Strain gauge F	1E0 - 1.5E2	E , ν	NTNU
	Takai et al. [80]	Polycrystals	PZT actuator	Load cells	Optical	1E-3 - 1 E1	E , Q_E^{-1}	UT
(ii) Torsional	Tsato and Madonna [102]	Sandstone	Motor	Load cell	Strain gauge cantilever	1E-1 - 1 E1	E , Q_E^{-1}	ETH
	Tsato et al. [113]	Sandstone	Motor	Load cell	Strain gauge	1E-1 - 2.5 E1	E , Q_E^{-1}	UofT
	Tsato et al. [242]	Marble	Motor	Load cell	Capacitive gap sensors	1E-1 - 1 E2	E , Q_E^{-1}	INGV
	Usher [65]	Various	Vibrators	Optical	Optical	2E0 - 4 E1	E , $\Delta W/W$	ICL
	Yee and Takemori [217]	Lucite	Hydraulic actuator	Load cell	Extensometer	1E-2 - 1.1 E1	E , Q_E^{-1}	GE
	Yurikov et al. [90]	Sandstone	PZT actuator	Aluminium STD	Fibre optics	1E-1 - 2 E2	E , Q_E^{-1} , ν	CU
	Béhuira et al. [137]	Unknown	Spindle	Inductive transducer	Transducer	1E-2 - 8 E1	G , Q_G^{-1}	CSM
	Berckheuer et al. [243]	Various	Electromagnetic drivers	Inductive transducer	Inductive transducer	1E-3 - 1 E2	G , Q_G^{-1}	FU
	Lee et al. [244]	Various	Coils	Aluminium STD	Interferometer	1E-3 - 1 E1	Q_G^{-1}	UW
	Paffenholz and Burkhardt [79]	Various	PZC transducer	Aluminium STD	Inductive transducer	3E-3 - 1 E2	G , Q_G^{-1}	TUB
	Peschnick and Outerbridge [64]	Limestone	Pendulum	Transducer	Inductive transducer	4E0 - 1 E1	G , Q_G^{-1}	USGS
	Guéguen et al. [163]	Forsterite	Electromagnetic drivers	Photodiode	Photodiode	1E-5 - 1 E1	G , Q_G^{-1}	IPGS
(iii) Flexural	Jackson et al. [162]	Granite	Electromagnetic drivers	Elastic STD	Capacitive transducer	1E-3 - 1 E0	G , δ	ANU
	Saltiel et al. [164]	Granite	Electromagnetic drivers	Load cell	Capacitive transducer	1E-3 - 1 E2	G , Q_G^{-1}	LBL
	Ikeda et al. [81]	Fused silica	PZT actuators	Titanium STD	Capacitive sensor	1E-1 - 1 E1	E_F , Q_{EF}^{-1}	UT(A)
(iv) Volumetric	Jackson et al. [71]	Igneous rocks	Electromagnetic drivers	Elastic STD	Capacitive transducer	1E-3 - 1 E0	E_F , δ	ANU
	Woignard and Guéguen [73]	Igneous rocks	Electromagnetic drivers	Inductive transducer	Inductive transducer	2E-2 - 1 E1	Q_{EF}^{-1}	CNRS
	Adélinet et al. [70]	Basalt	Confining pump	Pressure sensor	Strain gauge F	1E-2 - 1 E-1	K , Q_K^{-1}	ENS
(v) Uniaxial	Borgomano et al. [121]	Limestone	PZT actuator	Aluminium STD	Strain gauge F	4E-3 - 1.34E0	K , Q_K^{-1} , ν	ENS
	McCaun [245]	Water	PZT actuator	Pressure sensor	Load cell	1E-1 - 1 E2	K , Q_K^{-1}	UT(A)
	Pimienta et al. [169]	Sandstone	Confining pump	Pressure sensor	Strain gauge F	5E-3 - 5 E-1	K , Q_K^{-1}	ENS
	Lozovyi and Bauer [74]	Shale	PZT actuator	PZT transducer	Strain gauges F	1E-1 - 4 E0	C_{33}	NTNU
	Suarez-Rivera et al. [75]	Shale				1E0 - 2 E2	C_{33}	SINTEF

wider frequencies irrespective of material shape and dimensions. Be it extensional, torsional, and flexural modes, Zadler et al. [238] and Ulrich et al. [249] describe RUS as a technique able to ascertain the suite of elastic moduli for anisotropic rocks during a single frequency sweep (Figure 7). For orthorhombic symmetry, eight independent groups of free-vibration modes containing all possible combination of these symmetries (including isotropic, cubic, hexagonal, and tetragonal) exist: one extensional and torsional, plus three shear and flexural [248, 250]. RUS is as numerical as it is experimental in the sense that (i) forward and (ii) inverse problems need be solved to validate the experiment: (i) compute the frequencies and shapes of the normal modes, and (ii) apply a non-linear inversion algorithm to find the elastic constants from these normal-mode frequencies. Since RUS detects numerous resonance peaks from all eight groups, exact correspondence between resonance peaks and vibration modes is paramount as any dissonance make for erroneous measurements. Batzle et al. [33] remarked on RB versus RUS that the narrow bandwidth of RB limits the probed frequencies to the primary resonance and a few overtones whereas the extended frequencies of RUS renders it susceptible to jacketing and suspension procedures plus inhomogeneous strain conditions for the torsional and flexural modes. Indeed, Zadler et al. [238] acknowledged that *in-situ* measurements involving strong coupling to a pressurized medium violate the stress-free boundary conditions RUS is based upon.

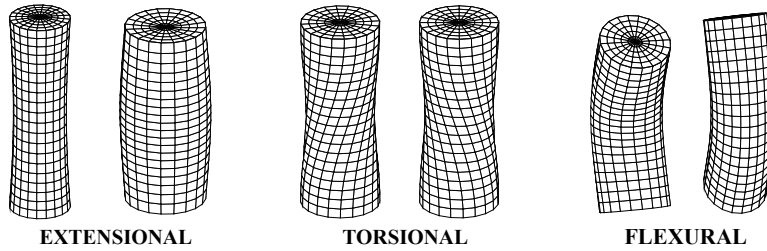


Figure 7 Exaggerated surface particle displacement for extensional, torsional, and flexural modes for RUS (but also applies to FO) measurements. Modified from Zadler et al. [238].

Harris [251] envisioned DARS to measure the change in resonance frequency of a submerged cavity caused by the absence or presence of a foreign object inside the cavity which perturbs the resonance properties of the cavity. DARS is based on perturbation theory which relates the frequency shift between a cavity with or without a specimen to the acoustic properties of said specimen [223, 252, 253]. In other words, DARS is restricted to the determination of bulk modulus as the change between the normal modes of two volumetric effects. Keys to this technique are (i) the cavity immersed in a fluid containing vessel, (ii) piezoceramic sources used to excite fluid resonances, and (iii) a hypersensitive hydrophone embedded on the cavity surface for detection of acoustic pressure signal changes. Added to these three key elements are also (iv) a computer-controlled step motor for accurate and repeatable specimen positioning, and (v) a phase-sensitive lock-in amplifier connected to source and receiver that uses a predefined frequency sweep (around the natural resonance of the cavity) to select the resonance curve of the fundamental mode in order to recognize the received signal at a specific reference frequency and phase. Wang et al. [252] implemented a FEM-based simulation to better understand the DARS system and improve its accuracy in estimating acoustic properties.

Scruby et al. [254] first described LUS as a technique to “study thermoelastic generation of elastic waves in a metal by unfocused laser radiation.” As such, LUS is able to characterize waves in terms of velocity and attenuation. Instead of relying on mechanical coupling between transducer and specimen like PT and FO, LUS is strictly non-contact due to two

lasers generating and recording elastic waves at the specimen surface from afar. A short pulse of electromagnetic radiation delivered by the first laser causes thermoelastic-expansion-induced ultrasonic waves recorded by the second laser (interferometer) at an arbitrary point on the specimen surface [255]. Since the surface area beamed by the laser is significantly smaller than the area coupled to PZT transducers, LUS enables multidirectional characterisation of waves from a single specimen while also guaranteeing that group velocity is unambiguously measured. The eternal group versus phase velocity conundrum is thus avoided as the former is easily converted to the latter using established algorithms. It is also claimed that the non-contact generation and detection is not frequency-limited by the physical dimensions of the transducer elements [256–258] yet it is curious that this possibility remains unexplored as most studies are limited to ultrasonic frequencies (thus the name) considering that seismic frequencies are alpha and omega in practice. If LUS is indeed universal for all frequencies, RB, PT, and FO would all be redundant. However, even if LUS is theoretically able but practically unable to probe all frequencies, it is still an improvement compared to PT because LUS leaves less ultrasonic frequencies unprobed. In the realm of rocks, PT measured parameters at ultrasonic frequencies are often regarded to coincide with the high-frequency limit but this need not be true and could be further explored by LUS. For example, there is evidence for ultrasonic attenuation in rocks depending on the enforced conditions (e.g. Johnston and Toksöz [259]). Simpson et al. [258], Scales and Malcolm [260], Lebedev et al. [261], Blum et al. [262], Carson and Lebedev [263], Adam et al. [264], Xie et al. [265], Adam et al. [266], Xie et al. [267], Simpson et al. [268], Adam et al. [269], and Simpson et al. [270] extended LUS from metals to rocks in the absence and (recently) in the presence of *pseudo in-situ* conditions. *Pseudo* is emphasized since it is still restricted to isotropic stress conditions but remain unrestricted in terms of temperature [258, 268, 270].

4 DISCUSSION

Technique-bias currently exists because several different techniques need be exploited to access Hz, kHz, and MHz frequencies. These techniques also measure different parameters that need be transformed for comparability which is in itself is an error source. Only if theoretically understood in a controlled environment (laboratory) may dispersion also be practically understood in an uncontrolled environment (field). To the end of understanding dispersion as a phenomenon, all frequencies need be accessible for the transitions between regimes to be studied. These transitions are mechanism-dependent and observed as changes in moduli or attenuation peaks with frequency. Dispersion and attenuation are indeed causality-bound. They are also key to identify and understand the physical mechanisms causing dispersion. Multiple transitions probably occur in any given rock but singular transitions are mostly studied due to frequency-limitations of the investigation techniques. The limiting factors for FO, RB, and PT are resonances (upper boundary), specimen size, and piezoceramic size, respectively. Resonances are constructive for RB and destructive for FO but the same principle applies to both: The smaller (and lighter) the resonator, the higher the characteristic frequency, and vice versa. In fact, this principle also applies to PT where larger piezoceramics equal lower frequency. PT piezoceramics for this purpose seldom recede below ~ 50 kHz. No universal technique probing all frequencies of interest alas exists at this time. As a result, existing techniques are enhanced or manipulated to extend their operating frequencies. For example, FO apparatuses are becoming smaller and lighter to increase the upper boundary at which they resonates. Numerical investigations during the design process accelerated this evolution. Batzle et al. [33] identified nodes and antinodes to extend this upper boundary by distributing the measurements accordingly. Since dispersion is a fluid-dependent phenomenon, viscosity-manipulation either by fluids such as glycerine [33,

103, 122, 129, 131, 145, 168–170, 218] or temperature [33, 50, 107, 190] may shift the transition from unprobed to probed frequencies due to altered fluid mobility. Viscosity-manipulation by temperature [271] is explored at high but unexplored at low temperatures for FO. Among RUS, LUS, and DARS, particularly LUS is enticing due to its non-contact nature and its supposed ability to “generate acoustic energy” and “detect surface displacements over a broad frequency band (typically from continuous to GHz)” [256]. Even if LUS is unable to probe seismic frequencies it is proven to probe a wider range of ultrasonic frequencies than PT. Thus far only isotropic (hydrostatic) conditions are possible [258] but applying a load along the axis of two synchronized stepper motors above and below the specimen to achieve biaxial conditions while still preserving its rotation ability should be fairly simple. Since most of the sensors are outside the pressure vessel, it is also an ideal candidate to fit inside a CT scanner provided that the laser signals are not somehow distorted by x-rays. “A respectable frequency gap remains to be bridged” [18] are still true words that are becoming less so with time and technological advancements.

Models compensate for the unprobed frequencies and also connect different measurements at different frequencies. Commonest amongst a multitude of models are CC, SLS, and KKR. KKR is superior to CC and SLS due to its analytical nature but requires parameters (real part) and their corresponding attenuations (imaginary part) at all frequencies to be valid. Many WIFF models based on Biot [25] exist because “squirt-flow” is the dominant dispersion mechanisms at microscopic scale in sandstones. Models simulating dispersive behaviour related to mechanisms valid at mesoscopic and macroscopic scales are rarities in comparison. Since multiple transitions may occur in the same specimen, it is important to simulate mesoscopic and macroscopic flows in addition to microscopic flow. As described in Section 3, not only analytical but also numerical models are developed to describe these mechanisms. The paucity of bound water models is concerning because it is perhaps the least known yet also the most critical mechanism due to its experimentally [272–275] and numerically [276] proven non-zero shear modulus and enhanced viscosity. DRP is progressing and may be a valuable tool in the future. Calibrating DRP with 3D printed or otherwise synthetic specimens with known geometry and properties would surely be a great leap forward if it becomes a possibility. More knowns than unknowns is key.

Subramaniyan et al. [7] is also a precautionary tale that discusses potential problems and possible solutions with implementing FO. As such, advantages and disadvantages with different components as well as boundary effects and strain amplitudes are discussed. Rørheim and Holt [6] discovered that moduli is unaffected but attenuation is affected by minor misalignments as foreseen by Liu and Peselnick [77]: smooth and parallel surfaces are paramount. For longitudinal excitation, deviatoric stress $\sigma_{\text{dev}} = \sigma_{\text{ax}} - P_c$ (where P_c is the previously undefined confining pressure) can be a mitigation measure to ensure adequate coupling and uniform stress distribution. Other mitigation measures include adhesive [21] and aluminum foil [158] at the specimen-endcap interfaces. FO apparatuses differ in primarily strain and secondary stress measurements. Most measure local strains using a set of specimen-attached strain gauges while few measure bulk strain using capacitors, cantilevers, lasers, or recently even fibre optics DAS sensors. *Pro et contra* of bulk versus local measurements are elaborated (Section 3) where bulk is considered superior to local (especially for heterogeneous rocks) but more problematic for radial measurements due to the double-interface problem. Strain gauges are more directional-versatile and require less calibration than the others but must be mounted to each individual specimen where the wires cause sealing-related problems. DAS is particularly interesting as it offers the opportunity to bridge the laboratory-field void because equivalent sensors are used in both environments. Mechanisms can thus be studied independent of potential sensor-bias. DAS is also more strain-sensitive (as low as 10^{-11} strain amplitudes) and less temperature-sensitive

than semiconductors among several advantages [90].

FO as a measure to probe seismic frequencies is a force to be reckoned with manifested by the growing number of apparatuses. Most of which are based on the design of Batzle et al. [33] with specimen-attached strain gauges for local strain measurements opposed to specimen-unattached transducers for bulk strain measurements like Spencer [21]. Simultaneous local and bulk strain measurements combined in one apparatus could possibly distinguish between microscopic, mesoscopic, and macroscopic mechanisms as dispersion and attenuation sources [85]. Other possible FO improvements for the future include:

- Numerical-based designs using, for example, COMputer SOLution (COMSOL) or Multiphysics Object Oriented Simulation Environment (MOOSE) framework are crucial in understanding the nature of resonance and predicting their nodal and antinodal distributions with frequency. Be it DRP or otherwise, numerical studies complementing experimental ones are also advancing the universal understanding of dispersion and attenuation mechanisms.
- Tisato et al. [113] was the first of its kind but others will surely follow because the CT-FO combination may elucidate the spatial distribution of fluids and thus also the fluid-solid interactions that are the dispersion and attenuation causing mechanisms. Most phenomena and their respective mechanisms are explained if porosity is adequately described as it is the critical factor separating solid and porous media. Measuring physical properties while simultaneous imaging phase distributions at pore-scale is common for other techniques [277] except FO. 3D printed or otherwise synthetic rock specimens with known geometry and properties subject to CT plus FO could also contribute to this end. Fractals may also be experimentally investigated if specimen geometries are scale-independent and fractal-consistent.
 - Imaging fluid-solid interactions with time is especially enticing for Carbon Capture and Storage (CCS) purposes (as a natural extension to Rørheim et al. [189]).
- Multi-element PZT transducers could also excite torsional and flexural modes as well as mitigate any potential misalignments by redistributing the stress field. Nakagawa [105] partially converted longitudinal into torsional excitations using a novel “compression-torsion coupler”. Misalignment mitigation and stress field redistribution is already achieved by employing three PZT transducers [79–81].
- True triaxial conditions ($\sigma_x \neq \sigma_y \neq \sigma_z$) [278, 279] are achieved if there is independent control of two radial strains in which $H = C_{11}$ in Equation 7. Pistons in addition to confining pressure are required to achieve these conditions which render specimen-attached strain gauges inadequate due to the fact that they would be destroyed upon impact of the piston. A cantilever solution in both axial and radial directions could however be a possibility.
- Virtual instead of physical lock-in amplifiers [108, 216] would offer greater data control as well as being an inexpensive option to split strain gauge elements to focus on local pore-scale processes by analyzing individual strains before averaging to distinguish local from global flow.
- Temperature control by heating circulators would render experimental temperature independent from laboratory temperature which is sensitive. Improved temperature control would not only allow for unexplored (sub- as well as superambient) temperatures to be explored but also keep the temperature constant for the duration of the experiment. Subambient temperatures are an unexplored curiosity shifting the mechanism-dependent transitions towards lower frequencies due to decreased fluid mobility.
- Machine Learning (ML) is bound to somehow be exploited in the laboratory as it is in the field [280] to ease data acquisition as well as analysis. PT is perhaps favoured over

FO though as automated arrival time picking ML is an immediate extension of Zhu and Beroza’s **PhaseNet**. Especially S-waves could benefit from automated picking due to their ambiguity compared to P-waves. ML could also possibly be combined with DRP.

5 CONCLUSION

Novel experimental techniques need be developed or enhanced to improve the conditions at which rocks are experimented for the field-laboratory gap to be bridged. Among the usual techniques, FO is perhaps the current champion due to its similarities with field seismic. Despite its promise, caution need be exercised when comparing laboratory with field data due to the omnipresent upscaling problem that transcends frequencies. Novel are not only the experimental techniques but also the analytical and numerical models that are continuously being developed. These models primarily describe WIFF at microscopic scale but secondary models to describe flows at mesoscopic and macroscopic are required for full understanding since multiple transitions are measured in rocks. Bound water should also be further explored as a mechanism due to its experimentally and numerically proven non-zero shear modulus and enhanced viscosity. DRP is gaining momentum and may possibly be integral in understanding rock phenomena and mechanisms in the future.

ACKNOWLEDGEMENTS

Rune M. Holt and Andrew J. Carter at NTNU are acknowledged for their encouragements. Current and former SINTEF employees are also acknowledged: Andreas Bauer, Jørn F. Stenebråten, Serhii Lozovyi, Dawid Szewczyk, Lars Erik Walle, Andreas N. Berntsen, Eyvind F. Sønstebø, M. Hossain Bhuiyan, Anna M. Stroisz, Pierre R. Cerasi, and Sigurd Bakheim. Lara Blazevic is finally acknowledged for proofreading.

BIBLIOGRAPHY

- [1] White, J.E., Martineau-Nicoletti, L., and Monash, C. “Measured anisotropy in Pierre shale”. In: *Geophysical Prospecting* 31.5 (1983), pp. 709–725.
- [2] Young, T. *A course of lectures on natural philosophy and the mechanical arts: in two volumes*. Vol. 2. Johnson, 1807.
- [3] Poisson, S.D. “Note sur l’extension des fils et des plaques élastiques”. In: *Annales de Chimie et de Physique*. Vol. 36. 1827, pp. 384–387.
- [4] Rørheim, S. “Frequency-dependent wave velocities in sediments and sedimentary rocks”. PhD thesis. Norwegian University of Science and Technology (NTNU), 2022.
- [5] Rørheim, S. “How can we approach the kHz range in laboratory rock physics?” In: NTNU ROSE Consortium, Apr. 2017.
- [6] Rørheim, S. and Holt, R.M. “How to avoid pitfalls in laboratory measured seismic attenuation”. In: *AGU Fall Meeting 2019*. AGU. 2019.
- [7] Subramaniyan, S., Quintal, B., Tisato, N., Saenger, E. H., and Madonna, C. “An overview of laboratory apparatuses to measure seismic attenuation in reservoir rocks”. In: *Geophysical Prospecting* 62.6 (2014), pp. 1211–1223. ISSN: 1365-2478. DOI: 10.1111/1365-2478.12171.

- [8] Bourbié, T. and Zinszner, B. “Hydraulic and acoustic properties as a function of porosity in Fontainebleau Sandstone”. In: *Journal of Geophysical Research: Solid Earth* 90.B13 (1985), pp. 11524–11532. DOI: 10.1029/JB090iB13p11524.
- [9] Kelvin, W. T. “Elements of a mathematical theory of elasticity”. In: *Philosophical Transactions of the Royal Society of London* 146 (1856), pp. 481–498.
- [10] Lamé, G. *Mémoire sur l’équilibre intérieur des corps solides homogènes*. 1833.
- [11] Hooke, R. *De Potentia Restitutiva*. John Martyn, London, 1678.
- [12] Hooke, R. “A Description of Helioscopes, and Some Other Instruments”. In: *Phil. Trans* (1675), pp. 440–2.
- [13] Einstein, A. “Die Grundlage der allgemeinen Relativitätstheorie”. In: *Annalen der Physik* 354.7 (1916), pp. 769–822. DOI: 10.1002/andp.19163540702.
- [14] Voigt, W. *Lehrbuch der kristallphysik: (mit ausschluss der kristalloptik)*. B.G. Teubners Sammlung von Lehrbüchern auf dem Gebiete der mathematischen Wissenschaften ; Bd. XXXIV. B.G. Teubner, 1910.
- [15] Mavko, Gary, Mukerji, Tapan, and Dvorkin, Jack. *The rock physics handbook*. Cambridge, United Kingdom: Cambridge university press, 2020. ISBN: 9781108420266.
- [16] Birch, F. “The velocity of compressional waves in rocks to 10 kilobars: 2.” In: *Journal of Geophysical Research* 66.7 (1961), pp. 2199–2224.
- [17] Gassmann, F. “Über die elastizität poröser medien: Vier. der Natur”. In: *Gesellschaft Zürich* 96 (1951), pp. 1–23.
- [18] Birch, F. and Bancroft, D. “Elasticity and internal friction in a long column of granite”. In: *Bulletin of the Seismological Society of America* 28.4 (1938), pp. 243–254.
- [19] Knopoff, L. “Q”. In: *Reviews of Geophysics* 2.4 (), pp. 625–660. DOI: <https://doi.org/10.1029/RG002i004p00625>.
- [20] O’Connell, R.J. and Budiansky, B. “Measures of dissipation in viscoelastic media”. In: *Geophysical Research Letters* 5.1 (1978), pp. 5–8. DOI: 10.1029/GL005i001p00005.
- [21] Spencer, J.W. “Stress relaxations at low frequencies in fluid-saturated rocks: Attenuation and modulus dispersion”. In: *Journal of Geophysical Research: Solid Earth* 86.B3 (1981), pp. 1803–1812. ISSN: 2156-2202. DOI: 10.1029/JB086iB03p01803.
- [22] Morozov, I.B. “Mechanics of seismic Q ”. In: *Recorder* 44 (1 2019).
- [23] Winkler, K.W. and Nur, A. “Pore fluids and seismic attenuation in rocks”. In: *Geophysical Research Letters* 6.1 (1979), pp. 1–4. DOI: 10.1029/GL006i001p00001.
- [24] Johnston, D.H., Toksöz, M.N., and imur, A. “Attenuation of seismic waves in dry and saturated rocks: II. Mechanisms”. In: *GEOPHYSICS* 44.4 (1979), pp. 691–711. DOI: 10.1190/1.1440970.
- [25] Biot, M.A. “Theory of Propagation of Elastic Waves in a Fluid-Saturated Porous Solid. I. Low-Frequency Range”. In: *The Journal of the Acoustical Society of America* 28.2 (1956), pp. 168–178. DOI: 10.1121/1.1908239.
- [26] White, J.E. “Computed seismic speeds and attenuation in rocks with partial gas saturation”. In: *Geophysics* 40.2 (1975), pp. 224–232.
- [27] Biot, M.A. “Mechanics of deformation and acoustic propagation in porous media”. In: *Journal of applied physics* 33.4 (1962), pp. 1482–1498.

- [28] Müller, T.M., Gurevich, B., and Lebedev, M. “Seismic wave attenuation and dispersion resulting from wave-induced flow in porous rocks - A review”. In: *GEOPHYSICS* 75.5 (2010), 75A147–75A164. DOI: 10.1190/1.3463417.
- [29] Tisato, N., Quintal, B., Chapman, S., Podladchikov, Y., and Burg, J.-P. “Bubbles attenuate elastic waves at seismic frequencies: First experimental evidence”. In: *Geophysical Research Letters* 42.10 (2015), pp. 3880–3887. DOI: 10.1002/2015GL063538.
- [30] Biot, M.A. “Theory of propagation of elastic waves in a fluid-saturated porous solid. II. Higher frequency range”. In: *The Journal of the Acoustical Society of America* 28.2 (1956), pp. 179–191. DOI: 10.1121/1.1908241.
- [31] Rice, J.R. and Cleary, M.P. “Some basic stress diffusion solutions for fluid-saturated elastic porous media with compressible constituents”. In: *Reviews of Geophysics* 14.2 (1976), pp. 227–241.
- [32] Box, G.E.P. “Science and statistics”. In: *Journal of the American Statistical Association* 71.356 (1976), pp. 791–799.
- [33] Batzle, M.L., Han, D.-H., and Hofmann, R. “Fluid mobility and frequency-dependent seismic velocity - Direct measurements”. In: *GEOPHYSICS* 71.1 (2006), N1–N9. DOI: 10.1190/1.2159053.
- [34] Cole, K.S. and Cole, R.H. “Dispersion and Absorption in Dielectrics I. Alternating Current Characteristics”. In: *The Journal of Chemical Physics* 9.4 (1941), pp. 341–351. DOI: 10.1063/1.1750906.
- [35] Zener, C. *Elasticity and anelasticity of metals*. University of Chicago press, 1948.
- [36] Kronig, R.d.L. “On the theory of dispersion of x-rays”. In: *Josa* 12.6 (1926), pp. 547–557.
- [37] Kramers, H.A. “La diffusion de la lumiere par les atomes”. In: *Atti Cong. Intern. Fisica (Transactions of Volta Centenary Congress) Como*. Vol. 2. 1927, pp. 545–557.
- [38] Debye, P.J.W. *Polar molecules*. Dover publications, 1929.
- [39] Maxwell, J.C. “On the dynamical theory of gases”. In: *Philosophical transactions of the Royal Society of London* 157 (1867), pp. 49–88.
- [40] Kelvin, W. T. “On the elasticity and viscosity of metals”. In: *Proc. Roy. Soc. London A* 14.289-297 (1865), p. 1.
- [41] Voigt, W. “Ueber innere Reibung fester Körper, insbesondere der Metalle”. In: *Annalen der Physik* 283.12 (1892), pp. 671–693.
- [42] Burgers, J.M. “First report on viscosity and plasticity”. In: *Nordemann Pub., New York* (1935).
- [43] Mikhaltsevitch, V.T., Lebedev, M., and Gurevich, B. “Validation of the laboratory measurements at seismic frequencies using the Kramers-Kronig relationship”. In: *Geophysical Research Letters* 43.10 (2016), pp. 4986–4991.
- [44] Ide, J.M. “Some Dynamic Methods for Determination of Young’s Modulus”. In: *Review of Scientific Instruments* 6.10 (1935), pp. 296–298. DOI: 10.1063/1.1751876.
- [45] Cady, W. G. “The Piezo-Electric Resonator”. In: *Proceedings of the Institute of Radio Engineers* 10.2 (Apr. 1922), pp. 83–114. DOI: 10.1109/JRPROC.1922.219800.
- [46] Quimby, S. L. “On the Experimental Determination of the Viscosity of Vibrating Solids”. In: *Phys. Rev.* 25 (4 Apr. 1925), pp. 558–573. DOI: 10.1103/PhysRev.25.558.

- [47] Boyle, R. W. and Sproule, D. O. "VELOCITY OF LONGITUDINAL VIBRATION IN SOLID RODS (ULTRASONIC METHOD) WITH SPECIAL REFERENCE TO THE ELASTICITY OF ICE". In: *Canadian Journal of Research* 5.6 (1931), pp. 601–618. DOI: 10.1139/cjr31-098.
- [48] Born, W.T. "The Attenuation Constant of Earth Materials". In: *GEOPHYSICS* 6.2 (1941), pp. 132–148. DOI: 10.1190/1.1443714.
- [49] Wang, Z. "3. Seismic Properties of Carbonate Rocks". In: *Carbonate Seismology*. 1997, pp. 29–52. DOI: 10.1190/1.9781560802099.ch3.
- [50] Jones, T. and Nur, A. "Velocity and attenuation in sandstone at elevated temperatures and pressures". In: *Geophysical Research Letters* 10.2 (1983), pp. 140–143. DOI: 10.1029/GL010i002p00140.
- [51] Winkler, K.W. and Nur, A. "Seismic attenuation: Effects of pore fluids and frictional-sliding". In: *GEOPHYSICS* 47.1 (1982), pp. 1–15. DOI: 10.1190/1.1441276.
- [52] Tittmann, B.R. "Internal Friction Measurements and their Implications in Seismic Q Structure Models of the Crust". In: *The Earth's Crust* (1977), pp. 197–213. DOI: 10.1029/GM020p0197.
- [53] Nakagawa, S. "Split Hopkinson resonant bar test for sonic-frequency acoustic velocity and attenuation measurements of small, isotropic geological samples". In: *Review of Scientific Instruments* 82.4 (2011), p. 044901. DOI: <http://dx.doi.org/10.1063/1.3579501>.
- [54] Hopkinson, B. "A Method of Measuring the Pressure Produced in the Detonation of High Explosives or by the Impact of Bullets". In: *Philosophical Transactions of the Royal Society of London A: Mathematical, Physical and Engineering Sciences* 213.497-508 (1914), pp. 437–456. DOI: 10.1098/rsta.1914.0010.
- [55] Kolsky, H. "An Investigation of the Mechanical Properties of Materials at very High Rates of Loading". In: *Proceedings of the Physical Society. Section B* 62.11 (1949), p. 676.
- [56] Hughes, D.S., Pondrom, W.L., and Mims, R.L. "Transmission of Elastic Pulses in Metal Rods". In: *Phys. Rev.* 75 (10 May 1949), pp. 1552–1556. DOI: 10.1103/PhysRev.75.1552.
- [57] Hughes, D.S. and Jones, H.J. "Variation of elastic moduli of igneous rocks with pressure and temperature". In: *Geological Society of America Bulletin* 61.8 (1950), pp. 843–856.
- [58] Hughes, D.S. and Jones, H.J. "Elastic wave velocities in sedimentary rocks". In: *Eos, Transactions American Geophysical Union* 32.2 (1951), pp. 173–178.
- [59] Wyllie, M.R.J., Gregory, A.R., and Gardner, L.W. "Elastic wave velocities in heterogeneous and porous media". In: *Geophysics* 21.1 (1956), pp. 41–70.
- [60] Birch, F. "The velocity of compressional waves in rocks to 10 kilobars: 1." In: *Journal of Geophysical Research (1896-1977)* 65.4 (1960), pp. 1083–1102. DOI: 10.1029/JZ065i004p01083.
- [61] Toksöz, M.H., Johnston, D.H., and Timur, A. "Attenuation of seismic waves in dry and saturated rocks: I. Laboratory measurements". In: *GEOPHYSICS* 44.4 (1979), pp. 681–690. DOI: 10.1190/1.1440969.
- [62] Winkler, K.W. "Frequency dependent ultrasonic properties of high-porosity sandstones". In: *Journal of Geophysical Research: Solid Earth* 88.B11 (1983), pp. 9493–9499. ISSN: 2156-2202. DOI: 10.1029/JB088iB11p09493.

- [63] Bruckshaw, J. M. and Mahanta, P. C. "THE VARIATION OF THE ELASTIC CONSTANTS OF ROCKS WITH FREQUENCY*". In: *Geophysical Prospecting* 9 (1961), pp. 65–76. ISSN: 1365-2478. DOI: 10.1111/j.1365-2478.1961.tb01690.x.
- [64] Peselnick, L. and Outerbridge, W.F. "Internal friction in shear and shear modulus of Solenhofen limestone over a frequency range of 10^7 cycles per second". In: *Journal of Geophysical Research (1896-1977)* 66.2 (1961), pp. 581–588. DOI: 10.1029/JZ066i002p00581.
- [65] Usher, M. J. "ELASTIC BEHAVIOUR OF ROCKS AT LOW FREQUENCIES". In: *Geophysical Prospecting* 10.2 (1962), pp. 119–127. ISSN: 1365-2478. DOI: 10.1111/j.1365-2478.1962.tb02002.x.
- [66] Norton, J.T. "A torsion pendulum instrument for measuring internal friction". In: *Review of Scientific Instruments* 10.3 (1939), pp. 77–81.
- [67] Kê, T.-S. and Ross, M. "An Apparatus for Measurement of Extremely High Internal Friction". In: *Review of Scientific Instruments* 20.11 (1949), pp. 795–799.
- [68] Koppelman, J. "Über die bestimmung des dynamischen elastizitätsmoduls und des dynamischen schubmoduls im frequenzbereich von 10^{-5} bis 10^{-1} Hz". In: *Rheologica Acta* 1.1 (1958), pp. 20–28.
- [69] Winkler, K.W. and Murphy, W.F. "Acoustic velocity and attenuation in porous rocks". In: *Rock physics and phase relations. A Handbook of physical constants* (1995), pp. 20–34.
- [70] Adelinet, M., Fortin, J., Guéguen, Y., Schubnel, A., and Geoffroy, L. "Frequency and fluid effects on elastic properties of basalt: Experimental investigations". In: *Geophysical Research Letters* 37.2 (2010). DOI: 10.1029/2009GL041660.
- [71] Jackson, I., Schijns, H., Schmitt, D.R., Mu, J., and Delmenico, A. "A versatile facility for laboratory studies of viscoelastic and poroelastic behaviour of rocks". In: *Review of Scientific Instruments* 82.6 (2011), p. 064501.
- [72] Woïrgard, J., Amirault, J.-P., Chaumet, H., and De Fouquet, J. "Appareil de mesure du module d'élasticité et du frottement intérieur en flexion, à basse fréquence, sous vide entre 20 et 800° C". In: *Revue de Physique Appliquée* 6.3 (1971), pp. 355–359.
- [73] Woïrgard, J. and Guéguen, Y. "Elastic modulus and internal friction in enstatite, forsterite and peridotite at seismic frequencies and high temperatures". In: *Physics of the Earth and Planetary Interiors* 17.2 (1978), pp. 140–146. ISSN: 0031-9201. DOI: [https://doi.org/10.1016/0031-9201\(78\)90055-9](https://doi.org/10.1016/0031-9201(78)90055-9).
- [74] Lozovyi, S. and Bauer, A. "Velocity dispersion in rocks: A laboratory technique for direct measurement of P-wave modulus at seismic frequencies". In: *Review of Scientific Instruments* 90.2 (2019), p. 024501. DOI: 10.1063/1.5026969.
- [75] Suarez-Rivera, R., Wilson, S.M., Nakagawa, S., and Nes, O.M. "Frequency scaling for evaluation of shale and mudstone properties from acoustic velocities". In: (2001).
- [76] Liu, H.-P. "Driving-stress waveform and the determination of rock internal friction by the stress—strain curve method". In: *Geophysical Journal International* 63.2 (1980), pp. 567–572.
- [77] Liu, H.-P. and Peselnick, L. "Investigation of internal friction in fused quartz, steel, plexiglass, and westerly granite from 0.01 to 1.00 Hertz at 10^{-8} to 10^{-7} strain amplitude". In: *Journal of Geophysical Research: Solid Earth* 88.B3 (1983), pp. 2367–2379. ISSN: 2156-2202. DOI: 10.1029/JB088iB03p02367.

- [78] Peselnick, L. and Liu, H.-P. “2. Laboratory measurement of internal friction in rocks and minerals at seismic frequencies”. In: *Methods in Experimental Physics*. Vol. 24. Elsevier, 1987, pp. 31–56.
- [79] Paffenholz, J. and Burkhardt, H. “Absorption and modulus measurements in the seismic frequency and strain range on partially saturated sedimentary rocks”. In: *Journal of Geophysical Research: Solid Earth* 94.B7 (1989), pp. 9493–9507. ISSN: 2156-2202. DOI: 10.1029/JB094iB07p09493.
- [80] Takei, Y., Fujisawa, K., and McCarthy, C. “Experimental study of attenuation and dispersion over a broad frequency range: 1. The apparatus”. In: *Journal of Geophysical Research: Solid Earth* 116.B9 (2011), n/a–n/a. ISSN: 2156-2202. DOI: 10.1029/2011JB008382.
- [81] Ikeda, K., Goldfarb, E., and Tisato, N. “A new apparatus for measuring low-frequency attenuation: Low-Frequency Module”. In: *SEG Technical Program Expanded Abstracts 2020*. Society of Exploration Geophysicists, 2020, pp. 2560–2564.
- [82] Fortin, J., Pimienta, L.X., Guéguen, Y., Schubnel, A., David, E.C., and Adelinet, M. “Experimental results on the combined effects of frequency and pressure on the dispersion of elastic waves in porous rocks”. In: *The Leading Edge* 33.6 (2014), pp. 648–654.
- [83] Pimienta, L.X., Fortin, J., Borgomano, J.V.M., and Guéguen, Y. “Dispersions and attenuations in a fully saturated sandstone: Experimental evidence for fluid flows at different scales”. In: *The Leading Edge* 35.6 (2016), pp. 495–501.
- [84] Borgomano, J. “Dispersion des modules élastiques de carbonates saturés: étude expérimentale et modélisation”. PhD thesis. PSL Research University, 2018.
- [85] Chapman, S. and Quintal, B. “Numerical analysis of local strain measurements in fluid-saturated rock samples submitted to forced oscillations”. In: *GEOPHYSICS* 83.5 (2018), MR309–MR316. DOI: 10.1190/geo2018-0071.1.
- [86] Adam, L. “Elastic and visco-elastic laboratory properties in carbonates”. PhD thesis. Colorado School of Mines, 2009.
- [87] Tisato, N. “Experimental characterization of reservoir rocks and geotechnical materials: Low frequency attenuation, ultrasonic velocities and local pore pressure effects”. PhD thesis. ETH Zurich, 2013.
- [88] Hall, Edwin H et al. “On a new action of the magnet on electric currents”. In: *American Journal of Mathematics* 2.3 (1879), pp. 287–292.
- [89] Yurikov, A., Lebedev, M., Pevzner, R., Tertyshnikov, K., and Mikhaltsevich, V.T. “Laboratory measurements of elastic properties at seismic frequencies using DAS sensors”. In: *EAGE GeoTech 2021 Second EAGE Workshop on Distributed Fibre Optic Sensing*. Vol. 2021. 1. European Association of Geoscientists & Engineers. 2021, pp. 1–5.
- [90] Yurikov, A., Pevzner, R., Tertyshnikov, K., Mikhaltsevich, V.T., Gurevich, B., and Lebedev, M. “Laboratory measurements with DAS: A fast and sensitive tool to obtain elastic properties at seismic frequencies”. In: *The Leading Edge* 40.9 (2021), pp. 655–661.
- [91] Yurikov, A., Pevzner, R., Tertyshnikov, K., Mikhaltsevich, V.T., Gurevich, B., and Lebedev, M. “Laboratory measurements with DAS: Fast and sensitive tool to obtain rock properties at seismic frequencies”. In: *6th International Workshop on Rock Physics*. International Association of Rock Physicists, 2022.
- [92] Adam, L. and Batzle, M.L. “Elastic properties of carbonates from laboratory measurements at seismic and ultrasonic frequencies”. In: *The Leading Edge* 27.8 (2008), pp. 1026–1032. DOI: 10.1190/1.2967556.

- [93] Sun, C., Tang, G.Y., Fortin, J., Borgomano, J.V., and Wang, S. “Dispersion and attenuation of elastic wave velocities: impact of microstructure heterogeneity and local measurements”. In: *Journal of Geophysical Research: Solid Earth* (2020), e2020JB020132.
- [94] Lienert, B.R. and Manghnani, M.H. “The relationship between Q_E^{-1} and dispersion in extensional modulus, E”. In: *Geophysical Research Letters* 17.6 (1990), pp. 677–680. ISSN: 1944-8007. DOI: 10.1029/GL017i006p00677.
- [95] Yin, C.-S., Batzle, M. L., and Smith, B. J. “Effects of partial liquid/gas saturation on extensional wave attenuation in Berea sandstone”. In: *Geophysical Research Letters* 19.13 (1992), pp. 1399–1402. DOI: 10.1029/92GL01159.
- [96] Cherry, R.H., Spetzler, H.A., and Paffenholz, J. “A new wideband (1 mHz to 100 Hz) seismic spectrometer”. In: *Review of scientific instruments* 67.1 (1996), pp. 215–221.
- [97] Chelidze, T.L., Spetzler, H.A., and Sobolev, G.A. “Absorption of strain waves in porous media at seismic frequencies”. In: *pure and applied geophysics* 147.1 (1996), pp. 25–55.
- [98] Batzle, M., Hofmann, R., Han, D.-H., and Castagna, J. “Fluids and frequency dependent seismic velocity of rocks”. In: *The Leading Edge* 20.2 (2001), pp. 168–171.
- [99] Gautam, K. “Fluid effects on attenuation and dispersion of elastic waves”. MA thesis. Colorado School of Mines, 2003.
- [100] Hofmann, R. “Frequency dependent elastic and anelastic properties of clastic rocks”. PhD thesis. Colorado School of Mines, 2006.
- [101] Madonna, C., Tisato, N., Boutareaud, S., and Mainprice, D. “A new laboratory system for the measurement of low frequency seismic attenuation”. In: *SEG Technical Program Expanded Abstracts 2010*. 2010, pp. 2675–2680. DOI: 10.1190/1.3513397.
- [102] Tisato, N. and Madonna, C. “Attenuation at low seismic frequencies in partially saturated rocks: Measurements and description of a new apparatus”. In: *Journal of Applied Geophysics* 86 (2012), pp. 44–53. ISSN: 0926-9851. DOI: <https://doi.org/10.1016/j.jappgeo.2012.07.008>.
- [103] David, E.C. “The effect of stress, pore fluid and pore structure on elastic wave velocities in sandstones”. PhD thesis. Imperial College London, 2012.
- [104] Madonna, C. and Tisato, N. “A new Seismic Wave Attenuation Module to experimentally measure low-frequency attenuation in extensional mode”. In: *Geophysical Prospecting* 61.2 (2013), pp. 302–314. ISSN: 1365-2478. DOI: 10.1111/1365-2478.12015.
- [105] Nakagawa, S. “Low-frequency (< 100 Hz) dynamic fracture compliance measurement in the laboratory”. In: *47th US Rock Mechanics/Geomechanics Symposium*. American Rock Mechanics Association. 2013.
- [106] Tisato, N. and Quintal, B. “Measurements of seismic attenuation and transient fluid pressure in partially saturated Berea sandstone: evidence of fluid flow on the mesoscopic scale”. In: *Geophysical Journal International* 195.1 (2013), pp. 342–351. DOI: 10.1093/gji/ggt259.
- [107] Spencer, J.W. “Viscoelasticity of Ells River bitumen sand and 4D monitoring of thermal enhanced oil recovery processes”. In: *GEOPHYSICS* 78.6 (2013), pp. D419–D428. DOI: 10.1190/geo2012-0535.1.
- [108] Yao, Q. and Han, D.-H. “Progresses on velocity dispersion and wave attenuation measurements at seismic frequency”. In: *SEG Technical Program Expanded Abstracts 2013*. 2013, pp. 2883–2888. DOI: 10.1190/segam2013-1217.1.

- [109] Mikhaltsevitch, V.T., Lebedev, M., and Gurevich, B. “Measurements of the elastic and anelastic properties of sandstone flooded with supercritical CO₂”. In: *Geophysical Prospecting* 62.6 (2014), pp. 1266–1277. ISSN: 1365-2478. DOI: 10.1111/1365-2478.12181.
- [110] Spencer, J.W. and Shine, J. “Seismic wave attenuation and modulus dispersion in sandstones”. In: *GEOPHYSICS* 81.3 (2016), pp. D211–D231. DOI: 10.1190/geo2015-0342.1.
- [111] Chapman, S., Tisato, N., Quintal, B., and Holliger, K. “Seismic attenuation in partially saturated Berea sandstone submitted to a range of confining pressures”. In: *Journal of Geophysical Research: Solid Earth* 121.3 (2016), pp. 1664–1676.
- [112] Ma, X.Y., Wang, S.X., Zhao, J.G., and Yin, H.J. “Multiscale Measurement for Wave Dispersion in Consolidated Sandstones”. In: *78th EAGE Conference and Exhibition 2016*. Vol. 2016. 1. European Association of Geoscientists & Engineers. 2016, pp. 1–5.
- [113] Tisato, N., Zhao, Q., and Grasselli, G. “Experimental rock physics under micro-CT”. In: *SEG Technical Program Expanded Abstracts 2016*. 2016, pp. 3251–3255. DOI: 10.1190/segam2016-13949603.1.
- [114] Pimienta, L.X., Borgomano, J.V.M., Fortin, J., and Guéguen, Y. “Elastic dispersion and attenuation in fully saturated sandstones: Role of mineral content, porosity, and pressures”. In: *Journal of Geophysical Research: Solid Earth* 122.12 (2017), pp. 9950–9965.
- [115] Sun, C., Tang, G.Y., Dong, C.H., Zhao, J.G., and Wang, S.X. “Fluid saturation effect on the characteristic frequency and attenuation of tight sandstone”. In: *79th EAGE Conference and Exhibition 2017*. Vol. 2017. 1. European Association of Geoscientists & Engineers. 2017, pp. 1–5.
- [116] Sun, C., Tang, G., Zhao, J., Zhao, L., and Wang, S. “An enhanced broad-frequency-band apparatus for dynamic measurement of elastic moduli and Poisson’s ratio of rock samples”. In: *Review of Scientific Instruments* (2018).
- [117] Chapman, S., Borgomano, J.V.M., Yin, H., Fortin, J., and Quintal, B. “Forced oscillation measurements of seismic wave attenuation and stiffness moduli dispersion in glycerine-saturated Berea sandstone”. In: *Geophysical Prospecting* 67.4 (2019), pp. 956–968.
- [118] Yin, H., Borgomano, J.V.M., Wang, S., Tiennot, M., Fortin, J., and Guéguen, Y. “Fluid Substitution and Shear Weakening in Clay-Bearing Sandstone at Seismic Frequencies”. In: *Journal of Geophysical Research: Solid Earth* 124.2 (2019), pp. 1254–1272.
- [119] Chavez, R., Mikhaltsevitch, V.T., Lebedev, M., Gurevich, B., Vargas, E., and Vasquez, G. “Influence of the Creep Effect on the Low-Frequency Measurements of the Elastic Moduli of Sedimentary Rocks”. In: *81st EAGE Conference and Exhibition 2019*. 2019.
- [120] Li, H., Wang, D., Gao, J., Zhang, M., Wang, Y., Zhao, L., and Yang, Z. “Role of Saturation on Elastic Dispersion and Attenuation of Tight Rocks: An Experimental Study”. In: *Journal of Geophysical Research: Solid Earth* 125.4 (2020), e2019JB018513. DOI: 10.1029/2019JB018513.
- [121] Borgomano, J.V.M., Gallagher, A., Sun, C., and Fortin, J. “An apparatus to measure elastic dispersion and attenuation using hydrostatic and axial-stress oscillations under undrained conditions”. In: *Review of Scientific Instruments* 91.3 (2020), p. 034502.

- [122] Gallagher, A., Borgomano, J.V.M., C., Sun., and Fortin, J. “Comparison of the elastic properties of reservoir rocks in the field and the laboratory: link between seismic, sonic and ultrasonic measurements”. In: *EGU General Assembly Conference Abstracts*. 2020, p. 1335.
- [123] Sun, C., Borgomano, J.V.M., Fortin, J., and Wang, S. “Effect of Pore Collapse and Grain Crushing on the Frequency Dependence of Elastic Wave Velocities in a Porous Sandstone”. In: *Rock Mechanics and Rock Engineering* (2020), pp. 1–13.
- [124] Li, H., Zhao, L., Han, D.-H., Gao, J., Yuan, H., and Wang, Y. “Experimental study on frequency-dependent elastic properties of weakly consolidated marine sandstone: effects of partial saturation”. In: *Geophysical Prospecting* 68.9 (2020), pp. 2808–2824.
- [125] Ògúnsàmi, A., Jackson, I., Borgomano, J.V.M., Fortin, J., Sidi, H., Gerhardt, A., Gurevich, B., Mikhaltsevitch, V., and Lebedev, M. “Elastic properties of a reservoir sandstone: a broadband inter-laboratory benchmarking exercise”. In: *Geophysical Prospecting* (2020).
- [126] Zhao, L., Tang, G., Sun, C., Zhao, J., and Wang, S. “Dual attenuation peaks revealing mesoscopic and microscopic fluid flow in partially oil-saturated Fontainebleau sandstones”. In: *Geophysical Journal International* 224.3 (2021), pp. 1670–1683.
- [127] Chapman, S., Borgomano, J.V.M., Quintal, B., Benson, S.M., and Fortin, J. “Seismic Wave Attenuation and Dispersion Due to Partial Fluid Saturation: Direct Measurements and Numerical Simulations Based on X-Ray CT”. In: *Journal of Geophysical Research: Solid Earth* 126.4 (2021), e2021JB021643.
- [128] Tisato, N., Madonna, C., and Saenger, E.H. “Attenuation of seismic waves in partially saturated Berea sandstone as a function of frequency and confining pressure”. In: *Frontiers in Earth Science* 9 (2021), p. 220.
- [129] Han, X., Wang, S., Tang, G., Dong, C., He, Y., Liu, T., Zhao, L., and Sun, C. “Coupled effects of pressure and frequency on velocities of tight sandstones saturated with fluids: measurements and rock physics modeling”. In: *Geophysical Journal International* (2021).
- [130] He, Y.-X., Wang, S.X., Sun, C., Tang, G.Y., and Zhu, W. “Analysis of the frequency dependence characteristics of wave attenuation and velocity dispersion using a poroelastic model with mesoscopic and microscopic heterogeneities”. In: *Geophysical Prospecting* 69.6 (2021), pp. 1260–1281.
- [131] Ma, X.Y. “Velocity Dispersion in Sandstone Under Partially Saturated Conditions”. In: *82nd EAGE Annual Conference & Exhibition*. Vol. 2021. 1. European Association of Geoscientists & Engineers. 2021, pp. 1–5.
- [132] Riabokon, E., Poplygin, V., Turbakov, M., Kozhevnikov, E., Kobiakov, D., Guzev, M., and Wiercigroch, M. “Nonlinear Young’s Modulus of New Red Sandstone: Experimental Studies”. In: *Acta Mechanica Solida Sinica* (2021), pp. 1–11.
- [133] Lu, C. “Experimental Investigation of Rock Dynamic Geomechanical Properties at Seismic Frequencies”. PhD thesis. University of Alberta, 2021.
- [134] Chapman, S., Borgomano, J.V.M., Quintal, B., Benson, S.M., and Fortin, J. “Mass transfer between fluids as a mechanism for seismic wave attenuation: experimental evidence from water–CO₂ saturated sandstones”. In: *Geophysical Journal International* 230.1 (2022), pp. 216–234.

- [135] He, Y.-X., Wang, S., Xi, B., Tang, G., Yin, H., Zhao, L., Sun, C., and Ma, X. “Role of pressure and pore microstructure on seismic attenuation and dispersion of fluid-saturated rocks: laboratory experiments and theoretical modelling”. In: *Geophysical Journal International* (2022).
- [136] Adam, L., Batzle, M.L., and Brevik, I. “Gassmann’s fluid substitution and shear modulus variability in carbonates at laboratory seismic and ultrasonic frequencies”. In: *GEOPHYSICS* 71.6 (2006), F173–F183. DOI: 10.1190/1.2358494.
- [137] Behura, J., Batzle, M.L., Hofmann, R., and Dorgan, J. “Heavy oils: Their shear story”. In: *GEOPHYSICS* 72.5 (2007), E175–E183. DOI: 10.1190/1.2756600.
- [138] Adam, L., Batzle, M.L., Lewallen, K.T., and Wijk, K. van. “Seismic wave attenuation in carbonates”. In: *Journal of Geophysical Research: Solid Earth* 114.B6 (2009). B06208, n/a–n/a. ISSN: 2156-2202. DOI: 10.1029/2008JB005890.
- [139] Zhao, Z.J., Wang, W.S., Li, L., Wei, W., and Yin, Y. “Studies on dispersion of reservoir rocks using multi-band direct laboratory measurement methodology with μ -CT scanning”. In: *76th EAGE Conference and Exhibition 2014*. Vol. 2014. 1. European Association of Geoscientists & Engineers. 2014, pp. 1–5.
- [140] Zhao, Z.J., Wang, W.S., Yin, H., Ma, X., Yan, X., and Li, Z. “Multi-band direct laboratory measurement-based dispersion analysis on reservoir rocks, 3rd Int”. In: *Workshop on Rock Physics*. 2015, pp. 1–5.
- [141] Mikhaltsevitch, V.T., Lebedev, M., and Gurevich, B. “Laboratory measurements of the effect of fluid saturation on elastic properties of carbonates at seismic frequencies”. In: *Geophysical Prospecting* 64.4 (2016), pp. 799–809.
- [142] Borgomano, J.V.M., Pimienta, L.X., Fortin, J., and Guéguen, Y. “Dispersion and attenuation measurements of the elastic moduli of a dual-porosity limestone”. In: *Journal of Geophysical Research: Solid Earth* 122.4 (2017), pp. 2690–2711. ISSN: 2169-9356. DOI: 10.1002/2016JB-013816.
- [143] Mikhaltsevitch, V.T., Lebedev, M., Peruvukhina, M., and Gurevich, B. “The effect of the boundary conditions on the elastic moduli measurements at low frequencies: Experimental study”. In: *Proceedings of the 5rd International Workshop on Rock Physics*. 2019, pp. 1–2.
- [144] Mikhaltsevitch, V.T., Lebedev, M., Pervukhina, M., and Gurevich, B. “A Laboratory Study of the Effect of Boundary Conditions on the Elastic Moduli Measurements”. In: *81st EAGE Conference and Exhibition 2019*. Vol. 2019. 1. European Association of Geoscientists & Engineers. 2019, pp. 1–6.
- [145] Borgomano, J.V.M., Pimienta, L.X., Fortin, J., and Guéguen, Y. “Seismic dispersion and attenuation in fluid-saturated carbonate rocks: effect of microstructure and pressure”. In: *Journal of Geophysical Research: Solid Earth* 124.12 (2019), pp. 12498–12522.
- [146] Riabokon, E., Turbakov, M., Popov, N., Kozhevnikov, E., Poplygin, V., and Guzev, M. “Study of the Influence of Nonlinear Dynamic Loads on Elastic Modulus of Carbonate Reservoir Rocks”. In: *Energies* 14.24 (2021), p. 8559.
- [147] Mikhaltsevitch, V.T., Lebedev, M., Chavez, R., Pervukhina, M., Glubokovskikh, S., and Vargas Jr., E.A. “The dead volume effect on the elastic moduli measurements using the forced-oscillation method”. In: *Geophysical Prospecting* n/a.n/a (2022), n/a. DOI: <https://doi.org/10.1111/1365-2478.13173>.

- [148] Sun, C., Fortin, J., Borgomano, J.V.M., Wang, S., Tang, G., Bultreys, T., and Cnudde, V. “Influence of fluid distribution on seismic dispersion and attenuation in partially saturated limestone”. In: *Journal of Geophysical Research: Solid Earth* (), e2021JB023867.
- [149] Gallagher, A., Fortin, J., and Borgomano, J.V.M. “Seismic Dispersion and Attenuation in Fractured Fluid-Saturated Porous Rocks: An Experimental Study with an Analytic and Computational Comparison”. In: *Rock Mechanics and Rock Engineering* (2022), pp. 1–18.
- [150] Duranti, L., Ewy, R., and Hofmann, R. “Dispersive and attenuative nature of shales: multiscale and multifrequency observations”. In: *SEG Technical Program Expanded Abstracts 2005*. 2005, pp. 1577–1580. DOI: 10.1190/1.2147994.
- [151] Sarker, R. and Batzle, M.L. “Anisotropic elastic moduli of the Mancos B Shale- An experimental study”. In: *SEG Technical Program Expanded Abstracts 2010*. 2010, pp. 2600–2605. DOI: 10.1190/1.3513381.
- [152] Delle Piane, C., Madonna, C., Dewhurst, D., Saenger, E.H., and Raven, M. “Attenuation and physical properties of shales from the Canning Basin, Western Australia”. In: *1st International Workshop on Rock Physics*. International Association of Rock Physicists, 2011.
- [153] Delle Piane, C., Sarout, J., Madonna, C., Saenger, E. H., Dewhurst, D. N., and Raven, M. “Frequency-dependent seismic attenuation in shales: experimental results and theoretical analysis”. In: *Geophysical Journal International* 198.1 (2014), pp. 504–515. DOI: 10.1093/gji/ggu148.
- [154] Mikhaltsevitch, V.T., Lebedev, M., and Gurevich, B. “A Laboratory Study of the Elastic and Anelastic Properties of the Eagle Ford Shale”. In: *77th EAGE Conference and Exhibition 2015*. Vol. 2015. 1. European Association of Geoscientists & Engineers. 2015, pp. 1–5.
- [155] Huang, Q., Han, D.-H., and Li, H. “Laboratory measurement of dispersion and attenuation in the seismic frequency”. In: *SEG Technical Program Expanded Abstracts 2015*. 2015, pp. 3090–3094. DOI: 10.1190/segam2015-5909141.1.
- [156] Szweczyk, D., Bauer, A., and Holt, R.M. “Stress-dependent elastic properties of shales—laboratory experiments at seismic and ultrasonic frequencies”. In: *Geophysical Journal International* 212.1 (Sept. 2017), pp. 189–210. ISSN: 0956-540X. DOI: 10.1093/gji/ggx392.
- [157] Mikhaltsevitch, V.T. “Investigations of Elastic Properties of Isotropic and Anisotropic Rocks at Seismic Frequencies Using Forced-Oscillation Experiments”. PhD thesis. Curtin University, 2017.
- [158] Li, H., Han, D.-H., Gao, J., and Huang, Q. “Measurement preciseness analysis of stress-strain system at seismic frequencies”. In: *SEG Technical Program Expanded Abstracts 2017*. 2017, pp. 3621–3625. DOI: 10.1190/segam2017-17654744.1.
- [159] Lozovyi, S. “Seismic Dispersion and the Relation between Static and Dynamic Stiffness of Shales”. PhD thesis. Norwegian University of Science and Technology (NTNU), 2018.
- [160] Mikhaltsevitch, V.T., Lebedev, M., Chavez, R., Vargas, E., and Vasquez, G.F. “A Laboratory Forced-Oscillation Apparatus for Measurements of Elastic and Anelastic Properties of Rocks at Seismic Frequencies”. In: *Frontiers in Earth Science* 9 (2021), p. 155.
- [161] Peselnick, L., Liu, H.-P., and Harper, K. R. “Observations of details of hysteresis loops in westerly granite”. In: *Geophysical Research Letters* 6.9 (1979), pp. 693–696. DOI: 10.1029/GL006i009p00693.

- [162] Jackson, I., Paterson, M.S., Niesler, H., and Waterford, R.M. “Rock anelasticity measurements at high pressure, low strain amplitude and seismic frequency”. In: *Geophysical Research Letters* 11 (Dec. 1984), pp. 1235–1238. ISSN: 0094-8276. DOI: 10.1029/GL011i012p01235.
- [163] Guéguen, Y., Darot, M., Mazot, P., and Woïrgard, J. “ Q^{-1} of forsterite single crystals”. In: *Physics of the earth and planetary interiors* 55.3-4 (1989), pp. 254–258.
- [164] Saltiel, S., Selvadurai, P.A., Bonner, B.P., Glaser, S.D., and Ajo-Franklin, J.B. “Experimental development of low-frequency shear modulus and attenuation measurements in mated rock fractures: Shear mechanics due to asperity contact area changes with normal stress”. In: *Geophysics* 82.2 (2017), pp. M19–M36.
- [165] McCann, M.R., Tisato, N., and Spikes, K. “Low-frequency attenuation measurements of fluids”. In: *SEG Technical Program Expanded Abstracts 2019*. Society of Exploration Geophysicists, 2019, pp. 3598–3602.
- [166] Tisato, N. and Quintal, B. “Laboratory measurements of seismic attenuation in sandstone: Strain versus fluid saturation effects”. In: *GEOPHYSICS* 79.5 (2014), WB9–WB14. DOI: 10.1190/geo2013-0419.1.
- [167] Kutelnikova, M., Tisato, N., Jänicke, R., and Quintal, B. “Numerical modeling and laboratory measurements of seismic attenuation in partially saturated rock”. In: *GEOPHYSICS* 79.2 (2014), pp. L13–L20. DOI: 10.1190/geo2013-0020.1.
- [168] Subramaniyan, S., Quintal, B., Madonna, C., and Saenger, E.H. “Laboratory-based seismic attenuation in Fontainebleau sandstone: Evidence of squirt flow”. In: *Journal of Geophysical Research: Solid Earth* 120.11 (2015), pp. 7526–7535.
- [169] Pimienta, L.X., Fortin, J., and Guéguen, Y. “Bulk modulus dispersion and attenuation in sandstones”. In: *GEOPHYSICS* 80.2 (2015), pp. D111–D127. DOI: 10.1190/geo2014-0335.1.
- [170] Pimienta, L.X., Fortin, J., and Guéguen, Y. “Experimental study of Young’s modulus dispersion and attenuation in fully saturated sandstones”. In: *Geophysics* 80.5 (2015), pp. L57–L72.
- [171] Tisato, N., Zhao, Q., Biryukov, A., and Grasselli, G. “Experimental Rock Deformation under μ CT: two new apparatuses”. In: *Geoscience new horizons, Geoconvention 2015, Telus Convention Center, 4-8 May 2015, Calgary, AB Canada*. 2015.
- [172] Chapman, S., Quintal, B., Tisato, N., and Holliger, K. “Frequency scaling of seismic attenuation in rocks saturated with two fluid phases”. In: *Geophysical Journal International* 208.1 (2017), pp. 221–225.
- [173] Wei, Q., Wang, Y., Han, D.-H., Sun, M., and Huang, Q. “Combined effects of permeability and fluid saturation on seismic wave dispersion and attenuation in partially-saturated sandstone”. In: *Advances in Geo-Energy Research* 5.2 (2021).
- [174] Tan, W., Müller, T.M., Ba, J., Mikhaltsevitch, V.T., and Cao, C. “Drained-to-undrained transition of bulk modulus in fluid-saturated porous rock induced by dead volume variation”. In: *Geophysical Prospecting* 68.8 (2020), pp. 2494–2503.
- [175] Müller, T.M. and Sahay, P.N. “Generalized poroelasticity framework for micro-inhomogeneous rocks”. In: *Geophysical Prospecting* 64. Advances in Rock Physics (2016), pp. 1122–1134.
- [176] Sun, C., Tang, G., Zhao, J., Zhao, L., Long, T., Li, M., and Wang, S. “Three-dimensional numerical modelling of the drained/undrained transition for frequency-dependent elastic moduli and attenuation”. In: *Geophysical Journal International* 219.1 (2019), pp. 27–38.

- [177] Ikeda, K., Subramaniyan, S., Quintal, B., Goldfarb, E.J., Saenger, E.H., and Tisato, N. “Low-Frequency Elastic Properties of a Polyminerale Carbonate: Laboratory Measurement and Digital Rock Physics”. In: *Frontiers in Earth Science* 9 (2021), p. 40.
- [178] Mikhaltsevitch, V.T., Lebedev, M., Gurevich, B., Pervukhina, M., and Zandi, S. “Elastic anisotropy of the Wellington shale at seismic frequencies: Laboratory measurements”. In: *SEG Technical Program Expanded Abstracts 2016*. Society of Exploration Geophysicists, 2016, pp. 392–397.
- [179] Mikhaltsevitch, V.T., Lebedev, M., and Gurevich, B. “The Effect of Water Saturation on the Elastic Properties of the Wellington Shale at Seismic Frequencies”. In: *80th EAGE Conference and Exhibition 2018*. Vol. 2018. 1. European Association of Geoscientists & Engineers. 2018, pp. 1–5.
- [180] Mikhaltsevitch, V.T., Lebedev, M., Pervukhina, M., and Gurevich, B. “Seismic dispersion and attenuation in Mancos shale - laboratory measurements”. In: *Geophysical Prospecting* 69.3 (2021), pp. 568–585. DOI: <https://doi.org/10.1111/1365-2478.13056>.
- [181] Mikhaltsevitch, V.T., Lebedev, M., and Gurevich, B. “A laboratory study of the elastic anisotropy in the Mancos shale at seismic frequencies”. In: *SEG Technical Program Expanded Abstracts 2016*. Society of Exploration Geophysicists, 2016, pp. 3174–3178.
- [182] Mikhaltsevitch, V.T., Lebedev, M., and Gurevich, B. “Effects of water saturation on P-wave anisotropy in the Mancos shale at seismic frequencies”. In: *79th EAGE Conference and Exhibition 2017*. Vol. 2017. 1. European Association of Geoscientists & Engineers. 2017, pp. 1–5.
- [183] Szweczyk, D., Bauer, A., and R.M. Holt, R.M. “A new laboratory apparatus for the measurement of seismic dispersion under deviatoric stress conditions”. In: *Geophysical Prospecting* 64.4 (2016), pp. 789–798. ISSN: 1365-2478. DOI: 10.1111/1365-2478.12425.
- [184] Szweczyk, D., Holt, R.M., and Bauer, A. “The impact of saturation on seismic dispersion in shales — Laboratory measurements”. In: *GEOPHYSICS* 83.1 (2018), MR15–MR34. DOI: 10.1190/geo2017-0169.1.
- [185] Szweczyk, D. “Frequency dependent elastic properties of shales - Impact of partial saturation and stress changes”. PhD thesis. Norwegian University of Science and Technology (NTNU), 2017.
- [186] Lozovyi, S., Bauer, A., Giger, S., and Chakraborty, S. “Static vs. dynamic stiffness of shales: frequency and stress effects”. In: *52nd US Rock Mechanics/Geomechanics Symposium*. American Association of Rock Mechanics. 2018.
- [187] Lozovyi, S. and Bauer, A. “Static and dynamic stiffness measurements with Opalinus Clay”. In: *Geophysical Prospecting* 67.4-Rock Physics: from microstructure to seismic signatures (2019), pp. 997–1019.
- [188] Lozovyi, S. and Bauer, A. “From static to dynamic stiffness of shales: frequency and stress dependence”. In: *Rock Mechanics and Rock Engineering* 52.12 (2019), pp. 5085–5098.
- [189] Rørheim, S., Bhuiyan, M.H., Bauer, A., and Cerasi, P.R. “On the Effect of CO₂ on Seismic and Ultrasonic Properties: A Novel Shale Experiment”. In: *Energies* 14.16 (2021), p. 5007.
- [190] Rørheim, S., Bauer, A., and Holt, R.M. “On the low-frequency elastic response of Pierre Shale during temperature cycles”. In: *Geophysical Journal International* 228.2 (2021), pp. 1260–1280.

- [191] Quintal, B., Steeb, H., Frehner, M., and Schmalholz, S.M. “Quasi-static finite element modeling of seismic attenuation and dispersion due to wave-induced fluid flow in poroelastic media”. In: *Journal of Geophysical Research: Solid Earth* 116.B1 (2011).
- [192] Quintal, B., Frehner, M., Madonna, C., Tisato, N., Kuteynikova, M., and Saenger, E.H. “Integrated numerical and laboratory rock physics applied to seismic characterization of reservoir rocks”. In: *The Leading Edge* 30.12 (2011), pp. 1360–1367.
- [193] Quintal, B., Chapman, S., Tisato, N., and Paffenholz, J. “Numerical Analysis of Laboratory Attenuation Measurements”. In: *Poromechanics VI*. 2017, pp. 1642–1649.
- [194] Hunziker, J., Favino, M., Caspari, E., Quintal, B., Rubino, J.G., Krause, R., and Holliger, K. “Seismic attenuation and stiffness modulus dispersion in porous rocks containing stochastic fracture networks”. In: *Journal of Geophysical Research: Solid Earth* 123.1 (2018), pp. 125–143.
- [195] Quintal, B., Caspari, E., Holliger, K., and Steeb, H. “Numerically quantifying energy loss caused by squirt flow”. In: *Geophysical Prospecting* 67.8 (2019), pp. 2196–2212.
- [196] Alkhimenkov, Y., Caspari, E., Gurevich, B., Barbosa, N.D., Glubokovskikh, S., Hunziker, J., and Quintal, B. “Frequency-dependent attenuation and dispersion caused by squirt flow: Three-dimensional numerical study”. In: *GEOPHYSICS* 0.ja (2020), pp. 1–71. DOI: 10.1190/geo2019-0519.1.
- [197] Lissa, S., Barbosa, N.D., Caspari, E., Alkhimenkov, Y., and Quintal, B. “Squirt flow in cracks with rough walls”. In: *Journal of Geophysical Research: Solid Earth* 125.4 (2020), e2019JB019235.
- [198] Lissa, S., Ruf, M., Steeb, H., and Quintal, B. “Effects of crack roughness on attenuation caused by squirt flow in Carrara marble”. In: *SEG Technical Program Expanded Abstracts 2020*. Society of Exploration Geophysicists, 2020, pp. 2439–2443.
- [199] Lissa, S., Ruf, M., Steeb, H., and Quintal, B. *Seismic moduli dispersion and attenuation obtained using Digital Rock Physics*. Tech. rep. Copernicus Meetings, 2021.
- [200] Lissa, S., Ruf, M., Steeb, H., and Quintal, B. “Digital rock physics applied to squirt flow”. In: *Geophysics* 86.4 (2021), pp. 1–40.
- [201] Alkhimenkov, Y. and Quintal, B. “An accurate analytical model for squirt flow in anisotropic porous rocks-Part 1: Classical geometry”. In: *Geophysics* 87.2 (2021), pp. 1–81.
- [202] Alkhimenkov, Y. and Quintal, B. “The characteristic frequency of squirt flow in porous rocks”. In: *6th International Workshop on Rock Physics*. International Association of Rock Physicists, 2022.
- [203] Zhang, Y. and Toksöz, M. N. “Computation of dynamic seismic responses to viscous fluid of digitized three-dimensional Berea sandstones with a coupled finite-difference method”. In: *The Journal of the Acoustical Society of America* 132.2 (2012), pp. 630–640.
- [204] Das, V., Mukerji, T., and Mavko, G. “Numerical simulation of coupled fluid-solid interaction at the pore scale: A digital rock-physics technology”. In: *Geophysics* 84.4 (2019), WA71–WA81.
- [205] Jänicke, R., Quintal, B., Larsson, F., and Runesson, K. “Viscoelastic substitute models for seismic attenuation caused by squirt flow and fracture leak off”. In: *Geophysics* 84.4 (2019), WA183–WA189.

- [206] Balcewicz, M., Siegert, M., Gurriss, M., Ruf, M., Krach, D., Steeb, H., and Saenger, E.H. “Digital rock physics: A geological driven workflow for the segmentation of anisotropic Ruhr sandstone”. In: *Frontiers in Earth Science* 9 (2021), p. 493.
- [207] Liu, X., Tang, G., Dong, C., Sun, C., Wang, J., and Wang, S. “Numerical Modeling of Stress-Strain Oscillation Experiments Using the Finite Element Method”. In: *81st EAGE Conference and Exhibition 2019*. 2019.
- [208] Li, H., Lin, J., Gao, J., He, Y., Han, D.-H., and Zhao, L. “Precision analysis of forced-oscillation device: numerical modelling and experimental investigations”. In: *Journal of Geophysics and Engineering* (2020).
- [209] Brunner, W.M., Getting, I.C., and Spetzler, H.A. “Device for the independent verification of subresonant mechanical damping measurements”. In: *Review of scientific instruments* 74.4 (2003), pp. 2604–2610.
- [210] Bonner, B.P. Private Communication. Berkeley, CA, USA, 2019.
- [211] Flidner, C. and French, M. “Pore fluid controls on seismic attenuation in a greenschist facies metapelite”. In: *AGU Fall Meeting 2021*. AGU. 2021.
- [212] Katzmann, J., Musialak, J., and Steeb, H. “Characterizing Materials in the Frequency Domain: Validation Experiments”. In: *PAMM* 19.1 (2019), e201900362.
- [213] Lakes, R. *Viscoelastic Materials*. Cambridge University Press, 2009. DOI: 10.1017/CBO9780511626722.
- [214] Madonna, C., Tisato, N., Artman, B., and Saenger, E. H. “Laboratory Measurements of Seismic Attenuation from 0.01 to 100 Hz”. In: *73rd EAGE Conference and Exhibition incorporating SPE EUROPEC 2011*. May 2011. DOI: 10.3997/2214-4609.20149425.
- [215] McCann, M.R. “Low-frequency attenuation measurements of fluids”. MA thesis. University of Texas at Austin, 2019.
- [216] Yao, Q. “Velocity dispersion and wave attenuation in reservoir rocks”. PhD thesis. University of Houston, 2013.
- [217] Yee, A.F and Takemori, M.T. “Dynamic bulk and shear relaxation in glassy polymers. I. Experimental techniques and results on PMMA”. In: *Journal of Polymer Science: Polymer Physics Edition* 20.2 (1982), pp. 205–224.
- [218] Yin, H., Zhao, J., Tang, G., Zhao, L., Ma, X., and Wang, S. “Pressure and Fluid Effect on Frequency-Dependent Elastic Moduli in Fully Saturated Tight Sandstone”. In: *Journal of Geophysical Research: Solid Earth* 122.11 (2017), pp. 8925–8942. DOI: 10.1002/2017JB014244.
- [219] Cadoret, T., Marion, D., and Zinszner, B. “Influence of frequency and fluid distribution on elastic wave velocities in partially saturated limestones”. In: *Journal of Geophysical Research: Solid Earth* 100.B6 (1995), pp. 9789–9803. DOI: 10.1029/95JB00757.
- [220] Cadoret, T., Mavko, G., and Zinszner, B. “Fluid distribution effect on sonic attenuation in partially saturated limestones”. In: *GEOPHYSICS* 63.1 (1998), pp. 154–160. DOI: 10.1190/1.1444308.
- [221] Gardner, G.H.F., Wyllie, M.R.J., and Droschak, D.M. “Effects of pressure and fluid saturation on the attenuation of elastic waves in sands”. In: *Journal of Petroleum Technology* 16.2 (1964). DOI: doi:10.2118/721-PA.
- [222] Goldberg, D. and Zinszner, B. “P-wave attenuation measurements from laboratory resonance and sonic waveform data”. In: *GEOPHYSICS* 54.1 (1989), pp. 76–81. DOI: 10.1190/1.1442579.

- [223] Harris, J.M., Quan, Y., and Xu, C. “Differential acoustical resonance spectroscopy: an experimental method for estimating acoustic attenuation of porous media”. In: *SEG Technical Program Expanded Abstracts 2005*. Society of Exploration Geophysicists, 2005, pp. 1569–1572.
- [224] Lucet, N., Rasolofosaon, P.N.J., and Zinszner, B. “Sonic properties of rocks under confining pressure using the resonant bar technique”. In: *The Journal of the Acoustical Society of America* 89.3 (1991), pp. 980–990. DOI: 10.1121/1.400643.
- [225] Lucet, N. and Zinszner, B. “Effects of heterogeneities and anisotropy on sonic and ultrasonic attenuation in rocks”. In: *GEOPHYSICS* 57.8 (1992), pp. 1018–1026. DOI: 10.1190/1.1443313.
- [226] Lucet, N. and Zinszner, B. “Frequency dependence of velocity in carbonate rocks”. In: *SEG Technical Program Expanded Abstracts 2006*. 2006, pp. 1898–1902. DOI: 10.1190/1.2369896.
- [227] McCann, C., Sothcott, J., and Best, A.I. “A new laboratory technique for determining the compressional wave properties of marine sediments at sonic frequencies and in situ pressures”. In: *Geophysical Prospecting* 62.1 (2014), pp. 97–116. DOI: 10.1111/1365-2478.12079.
- [228] Murphy, W.F. III. “Effects of partial water saturation on attenuation in Massillon sandstone and Vycor porous glass”. In: *The Journal of the Acoustical Society of America* 71.6 (1982), pp. 1458–1468. DOI: 10.1121/1.387843.
- [229] Murphy, W.F. “Acoustic measures of partial gas saturation in tight sandstones”. In: *Journal of Geophysical Research: Solid Earth* 89.B13 (1984), pp. 11549–11559. DOI: 10.1029/JB089iB13p11549.
- [230] Nakagawa, S. and Kneafsey, T.J. “Split Hopkinson Resonant Bar test and its application for seismic property characterization of geological media”. In: *44th US Rock Mechanics Symposium and 5th US-Canada Rock Mechanics Symposium*. American Rock Mechanics Association. 2010.
- [231] Nakagawa, S. and Kneafsey, T.J. *Application of the Split Hopkinson Resonant Bar Test for Seismic Property Characterization of Hydrate-bearing Sand Undergoing Water Saturation*. 2011. DOI: 10.2172/1052176.
- [232] O’Hara, S.G. “Influence of pressure, temperature, and pore fluid on the frequency-dependent attenuation of elastic waves in Berea sandstone”. In: *Phys. Rev. A* 32 (1 July 1985), pp. 472–488. DOI: 10.1103/PhysRevA.32.472.
- [233] Priest, J.A.; Best, A.I., and Clayton, C.R.I. “Attenuation of seismic waves in methane gas hydrate-bearing sand”. In: *Geophysical Journal International* 164.1 (2006), pp. 149–159.
- [234] Tittmann, B.R., Nadler, H., Clark, V.A., Ahlberg, L.A., and Spencer, T.W. “Frequency dependence of seismic dissipation in saturated rocks”. In: *Geophysical Research Letters* 8.1 (1981), pp. 36–38. DOI: 10.1029/GL008i001-p00036.
- [235] Waite, W., Santamarina, J., Rydzy, M., Chong, S.H., Grozic, J.L.H., Hester, K., Howard, J., Kneafsey, T.J., Lee, J.Y., Nakagawa, S., et al. “Inter-laboratory comparison of wave velocity measurements in a sand under hydrate-bearing and other set conditions”. In: *7th International Conference on Gas Hydrates*. 2011.
- [236] Wegel, R.L. and Walther, H. “Internal Dissipation in Solids for Small Cyclic Strains”. In: *Physics* 6.4 (1935), pp. 141–157. DOI: 10.1063/1.1745306.

- [237] Wyllie, M. R. J., Gardner, G.H.F., and Gregory, A. R. "STUDIES OF ELASTIC WAVE ATTENUATION IN POROUS MEDIA". In: *GEOPHYSICS* 27.5 (1962), pp. 569–589. DOI: 10.1190/1.1439063.
- [238] Zadler, B.J., Le Rousseau, J.H.L., Scales, J.A., and Smith, M.L. "Resonant Ultrasound Spectroscopy: theory and application". In: *Geophysical Journal International* 156.1 (2004), p. 154. DOI: 10.1111/j.1365-246X.2004.02093.x.
- [239] Fliedner, C. and French, M.E. "Anelasticity of the Orocopia schist under different effective pressures and temperatures." In: *AGU Fall Meeting 2019*. AGU. 2019.
- [240] Fortin, J., Schubnel, A., and Guéguen, Y. "Elastic wave velocities and permeability evolution during compaction of Bleurswiller sandstone". In: *International Journal of Rock Mechanics and Mining Sciences* 42.7 (2005). Rock Physics and Geomechanics, pp. 873–889. ISSN: 1365-1609. DOI: <https://doi.org/10.1016/j.ijrmms.2005.05.002>.
- [241] Li, M., Wang, D., and Zhao, Y. "Laboratory study of the elastic properties of sandstones at seismic and ultrasonic frequencies". In: *SEG Technical Program Expanded Abstracts 2019*. 2019, pp. 3613–3617. DOI: 10.1190/segam2019-3215346.1.
- [242] Tisato, N., Harbord, C., Spagnuolo, E., Di Stefano, G., and Di Toro, G. "A new apparatus to study visco-elastic properties in large displacement experimental faults". In: *AGU Fall Meeting 2019*. AGU. 2019.
- [243] Berckhemer, H., Kampfmann, W., Aulbach, E., and Schmeling, H. "Shear modulus and Q of forsterite and dunite near partial melting from forced-oscillation experiments". In: *Physics of the earth and planetary interiors* 29.1 (1982), pp. 30–41.
- [244] Lee, T., Lakes, R., and Lal, A. "Resonant ultrasound spectroscopy for measurement of mechanical damping: Comparison with broadband viscoelastic spectroscopy". In: *Review of Scientific Instruments* 71.7 (2000), pp. 2855–2861.
- [245] Maynard, J. "Resonant ultrasound spectroscopy". In: *Physics Today* 49.1 (1996), pp. 26–31.
- [246] Fraser, D.B. and LeCraw, R.C. "Novel method of measuring elastic and anelastic properties of solids". In: *Review of Scientific Instruments* 35.9 (1964), pp. 1113–1115.
- [247] Schreiber, E. and Anderson, O.L. "Properties and composition of lunar materials: Earth analogies". In: *Science* 168.3939 (1970), pp. 1579–1580.
- [248] Demarest, H.H.Jr. "Cube-resonance method to determine the elastic constants of solids". In: *The Journal of the Acoustical Society of America* 49.3B (1971), pp. 768–775.
- [249] Ulrich, T.J., McCall, K.R., and Guyer, R.A. "Determination of elastic moduli of rock samples using resonant ultrasound spectroscopy". In: *The Journal of the Acoustical Society of America* 111.4 (2002), pp. 1667–1674. DOI: 10.1121/1.1463447.
- [250] Ohno, I. "Free vibration of a rectangular parallelepiped crystal and its application to determination of elastic constants of orthorhombic crystals". In: *Journal of Physics of the Earth* 24.4 (1976), pp. 355–379.
- [251] Harris, J.M. *Differential Acoustic Resonance Spectroscopy, Seismic Tomography Project Annual Report, Paper F*. Stanford University, 1996.
- [252] Wang, S.-x., Zhao, J.-g., Li, Z.-h., Harris, J.M., and Quan, Y. "Differential Acoustic Resonance Spectroscopy for the acoustic measurement of small and irregular samples in the low frequency range". In: *Journal of Geophysical Research: Solid Earth* 117.B6 (2012).

- [253] Vogelaar, B.B.S.A., Smeulders, D.M.J., and Harris, J.M. “Theory and experiment of differential acoustic resonance spectroscopy”. In: *Journal of Geophysical Research: Solid Earth* 120.11 (2015), pp. 7425–7439.
- [254] Scruby, C.B., Dewhurst, R.J., Hutchins, D.A., and Palmer, S.B. “Quantitative studies of thermally generated elastic waves in laser-irradiated metals”. In: *Journal of Applied Physics* 51.12 (1980), pp. 6210–6216.
- [255] Scruby, C.B. and Drain, L.E. *Laser ultrasonics techniques and applications*. CRC press, 1990.
- [256] Pouet, B.F. and Rasolofosaon, P.N.J. “Seismic physical modeling using laser ultrasonics”. In: *SEG Technical Program Expanded Abstracts 1990*. Society of Exploration Geophysicists, 1990, pp. 841–844.
- [257] Pouet, B.F. and Rasolofosaon, P.N.J. “Measurement of broadband intrinsic ultrasonic attenuation and dispersion in solids with laser techniques”. In: *The Journal of the Acoustical Society of America* 93.3 (1993), pp. 1286–1292.
- [258] Simpson, J., Wijk, K. van, Adam, L., and Smith, C. “Laser ultrasonic measurements to estimate the elastic properties of rock samples under in situ conditions”. In: *Review of Scientific Instruments* 90.11 (2019), p. 114503.
- [259] Johnston, D.H. and Toksöz, M.N. “Ultrasonic P and S wave attenuation in dry and saturated rocks under pressure”. In: *Journal of Geophysical Research: Solid Earth* 85.B2 (1980), pp. 925–936.
- [260] Scales, J.A. and Malcolm, A.E. “Laser characterization of ultrasonic wave propagation in random media”. In: *Physical Review E* 67.4 (2003), p. 046618.
- [261] Lebedev, M., Bóna, A., Pevzner, R., and Gurevich, B. “Elastic anisotropy estimation from laboratory measurements of velocity and polarization of quasi-P-waves using laser interferometry”. In: *Geophysics* 76.3 (2011), WA83–WA89.
- [262] Blum, T.E., Adam, L., and Van Wijk, K. “Noncontacting benchtop measurements of the elastic properties of shales”. In: *Geophysics* 78.3 (2013), pp. C25–C31.
- [263] Carson, M. and Lebedev, M. “Ultrasonic measurements of S waves using laser interferometry”. In: *SEG Technical Program Expanded Abstracts 2014*. Society of Exploration Geophysicists, 2014, pp. 2755–2759.
- [264] Adam, L., Ou, F., Strachan, L., Johnson, J., Wijk, K. van, and Field, B. “Mudstone P-wave anisotropy measurements with non-contacting lasers under confining pressure”. In: *SEG Technical Program Expanded Abstracts 2014*. Society of Exploration Geophysicists, 2014, pp. 2749–2754.
- [265] Xie, J., Wei, J., Di, B., Xu, K., and Chen, Y. “Experimental and theoretical enhancement of the inversion accuracy of the Thomsen parameter δ in organic-rich shale”. In: *Journal of Geophysics and Engineering* 13.6 (2016), pp. 984–993.
- [266] Adam, L., Trimble, M., Barnhoorn, A., Houben, M.E., Strachan, L., and Field, B. “Seismic attenuation: Observations and mechanisms”. In: *4th International Workshop on Rock Physics*. International Association of Rock Physicists, 2017.
- [267] Xie, J., Di, B., Schmitt, D.R., Wei, J., and Chen, Y. “Estimation of δ and C13 of organic-rich shale from laser ultrasonic technique measurement”. In: *Geophysics* 83.4 (2018), pp. C137–C152.

- [268] Simpson, J., Adam, L., Wijk, K. van, and Charoensawan, J. “Constraining Microfractures in Foliated Alpine Fault Rocks With Laser Ultrasonics”. In: *Geophysical Research Letters* 47.8 (2020), e2020GL087378.
- [269] Adam, L., Frehner, M., Sauer, K., Toy, V., and Guerin-Marthe, S. “Seismic anisotropy and its impact on imaging the shallow Alpine Fault: an experimental and modeling perspective”. In: *Journal of Geophysical Research: Solid Earth* 125.8 (2020), e2019JB019029.
- [270] Simpson, J., Wijk, K. van, and Adam, L. “Spatial Dependence of Dynamic Nonlinear Rock Weakening at the Alpine Fault, New Zealand”. In: *Geophysical Research Letters* 48.14 (2021), e2021GL093862.
- [271] Batzle, M.L. and Wang, Z. “Seismic properties of pore fluids”. In: *GEOPHYSICS* 57.11 (1992), pp. 1396–1408. DOI: 10.1190/1.1443207.
- [272] Antognozzi, M., Humphris, A.D.L., and Miles, M.J. “Observation of molecular layering in a confined water film and study of the layers viscoelastic properties”. In: *Applied Physics Letters* 78.3 (2001), pp. 300–302.
- [273] Major, R.C., Houston, J.E., McGrath, M.J., Siepmann, J.I., and Zhu, X.-Y. “Viscous water meniscus under nanoconfinement”. In: *Physical review letters* 96.17 (2006), p. 177803.
- [274] Goertz, M.P., Houston, J.E., and Zhu, X.-Y. “Hydrophilicity and the viscosity of interfacial water”. In: *Langmuir* 23.10 (2007), pp. 5491–5497.
- [275] Ulcinas, A., Valdre, G., Snitka, V., Miles, M.J., Claesson, P.M., and Antognozzi, M. “Shear response of nanoconfined water on muscovite mica: role of cations”. In: *Langmuir* 27.17 (2011), pp. 10351–10355.
- [276] Holt, R.M. and Kolstø, M.I. “How does water near clay mineral surfaces influence the rock physics of shales?” In: *Geophysical Prospecting* 65.6 (2017), pp. 1615–1629.
- [277] Noiriél, C. and Renard, F. “Four-dimensional X-ray micro-tomography imaging of dynamic processes in geosciences”. In: *Comptes Rendus. Géoscience* 354.G2 (2022), pp. 255–280.
- [278] Walle, L.E., Berntsen, A.N., and Bauer, A. “Novel true triaxial apparatus applied to the study of thermal effects on water injectivity under anisotropic stress conditions”. In: *53rd US Rock Mechanics/Geomechanics Symposium*. American Association of Rock Mechanics. 2019.
- [279] Walle, L.E., Berntsen, A.N., and Papamichos, E. “Novel true triaxial apparatus applied to the study of sand mass production under anisotropic stress conditions.” In: *Rock Mechanics for Natural Resources and Infrastructure Development* (2019).
- [280] Zhu, W. and Beroza, G.C. “PhaseNet: a deep-neural-network-based seismic arrival-time picking method”. In: *Geophysical Journal International* 216.1 (Oct. 2018), pp. 261–273. ISSN: 0956-540X. DOI: 10.1093/gji/ggy423.

ACRONYMS

ANU	Australian National University.
CC	Cole-Cole.
CCS	Carbon Capture and Storage.
CNRS	Centre national de la recherche scientifique.

CO₂	Carbon dioxide.
COMSOL	COMputer SOLution.
CSM	Colorado School of Mines.
CT	Computed Tomography.
CU	Curtin University.
CUP	China University of Petroleum.
DARS	Differential Acoustic Resonance Spectroscopy.
DAS	Distributed Acoustic Sensing.
DRP	Digital Rock Physics.
ECP	Eddy Current Probe.
ENS	École Normale Supérieure (Paris).
ETH	Eidgenössische Technische Hochschule (Zürich).
FEM	Finite Element Method.
FFT	Fast Fourier Transform.
FO	Forced-Oscillation.
FU	Frankfurt University.
GE	General Electric.
GHRC	Gas Hydrate Resonant Column.
ICL	Imperial College London.
INGV	Istituto Nazionale de Geofisica e Vulcanologia.
IPGS	Institut de Physique du Globe de Strasbourg.
KKR	Kramers-Kronig relations.
LBL	Lawrence Berkeley National Laboratory.
LDS	Laser Displacement Sensors.
LUS	Laser UltraSonics.
LV	Laser Vibrometer.
LVDT	Linear Variable Displacement Transducer.
ML	Machine Learning.
MOOSE	Multiphysics Object Oriented Simulation Environment.
N₂	Dinitrogen.

NTNU	Norwegian University of Science and Technology.
PE	Pulse-Echo.
PEEK	Polyether Ether Ketone.
PT	Pulse-Transmission.
PTU	Pulse-Tube.
PZC	Piezoceramic.
PZT	Lead Zirconate Titanate (piezoceramic material).
RB	Resonant Bar.
RH	Relative Humidity.
RU	Rice University.
RUS	Resonant Ultrasound Spectroscopy.
SHPB	Split-Hopkinson Pressure Bar.
SHRB	Split-Hopkinson Resonance Bar.
SLS	Standard Linear Solid.
SR	Spectral Ratio.
TI	Transverse Isotropy.
TUB	Technische Universität Berlin.
UA	University of Aberdeen.
UCB	University of Colorado Boulder.
UH	University of Houston.
UofA	University of Alberta.
UofT	University of Toronto.
UoH	University of Hawaii.
US	University of Stuttgart.
USGS	United States Geological Survey.
UT	University of Tokyo.
UT(A)	University of Texas (at Austin).
UW	University of Wisconsin-Madison.
WIFF	Wave-Induced Fluid Flow.
WIGED	Wave-Induced Gas Exsolution Dissolution.

NOMENCLATURE

α	Cole-Cole's spreading factor.	$\in [0, 1]$
\overleftrightarrow{C}	Stiffness tensor.	
$\overrightarrow{\epsilon}$	Strain vector.	
$\overrightarrow{\sigma}$	Stress vector.	
$\Delta\theta$	Phase angle.	
Δt	Travel time.	
ΔW	Energy loss per cycle.	
ϵ	Strain.	
ϵ_{ax}	Axial strain.	
ϵ_{rad}	Radial strain.	
ϵ_{s}	Shear strain.	
ϵ_{vol}	Volumetric strain.	
ϵ_{11}	One of the strains ϵ_{ij} .	
ϵ_{12}	One of the strains ϵ_{ij} .	
ϵ_{13}	One of the strains ϵ_{ij} .	
ϵ_{22}	One of the strains ϵ_{ij} .	
ϵ_{23}	One of the strains ϵ_{ij} .	
ϵ_{33}	One of the strains ϵ_{ij} .	
ϵ_{kl}	Einstein notation for strain.	
η	Viscosity.	
λ	Wavelength.	
λ_{L}	Lamé's first parameter.	
μ_{L}	Lamé's second parameter.	
ν	Poisson's ratio.	
ν_{HH}	One of three Poisson's ratios assuming TI symmetry.	
ν_{HV}	One of three Poisson's ratios assuming TI symmetry.	
ν_{VH}	One of three Poisson's ratios assuming TI symmetry.	
π	Pi.	3.141592653...
ρ	Density.	

σ	Stress.
σ_{ax}	Axial stress.
σ_{dev}	Deviatoric stress.
σ_{p}	Hydrostatic stress (or pressure).
σ_{s}	Shear stress.
σ_{x}	One of the principal stresses in z -direction.
σ_{y}	One of the principal stresses in y -direction.
σ_{z}	One of the principal stresses in z -direction.
σ_{11}	One of the stresses σ_{ij} .
σ_{12}	One of the stresses σ_{ij} .
σ_{13}	One of the stresses σ_{ij} .
σ_{22}	One of the stresses σ_{ij} .
σ_{23}	One of the stresses σ_{ij} .
σ_{33}	One of the stresses σ_{ij} .
σ_{ij}	Einstein notation for stress.
θ_{SPE}	Specimen phase.
θ_{STD}	Standard phase.
θ_{ϵ}	Strain phase
θ_{σ}	Stress phase.
B_{SPE}	Strain amplitude of specimen.
B_{STD}	Strain amplitude of standard.
C_{11}	One of five stiffnesses assuming TI symmetry.
C_{13}	One of five stiffnesses assuming TI symmetry.
C_{33}	One of five stiffnesses assuming TI symmetry.
C_{33}	One of five stiffnesses assuming TI symmetry.
C_{44}	One of five stiffnesses assuming TI symmetry.
C_{66}	One of five stiffnesses assuming TI symmetry.
C_{ijkl}	Einstein notation for stiffnesses.
C_{ij}	Voigt notation for stiffnesses.
E	Young's modulus.

E_H	One of three Young's moduli assuming TI symmetry.
E_V	One of three Young's moduli assuming TI symmetry.
E_{45}	One of three Young's moduli assuming TI symmetry.
f	Resonant frequency.
G	Shear modulus.
H	Uniaxial (or P-wave) modulus.
K	Bulk modulus.
k	Permeability.
L	Specimen length.
M	Complex modulus.
M_{\Im}	Imaginary part of complex modulus M .
M_F	Fluid mobility.
M_{\Re}	Real part of complex modulus M .
n	Positive integer in which $n \in \{1, 2, 3, \dots\}$ representing nodes or harmonics.
P_c	Confining pressure.
Q	Quality factor.
Q^{-1}	Inverse quality factor.
$Q_{E_H}^{-1}$	Inverse quality factor of Young's modulus E_H assuming TI symmetry.
$Q_{E_V}^{-1}$	Inverse quality factor of Young's modulus E_V assuming TI symmetry.
$Q_{E_{45}}^{-1}$	Inverse quality factor of Young's modulus E_{45} assuming TI symmetry.
Q_E^{-1}	Inverse quality factor of Young's modulus E .
Q_G^{-1}	Inverse quality factor of shear modulus G .
Q_K^{-1}	Inverse quality factor of bulk modulus K .
Q_ν^{-1}	Inverse quality factor of Poisson's ratio ν .
u_r	Radial displacement.
u_z	Axial displacement.
u_θ	Circumferential displacement.
V	Velocity.
V_E	Longitudinal or flexural velocity.
V_G	Torsional velocity.

V_{P_0}	P-wave velocity normal to bedding.
$V_{P_{45}}$	P-wave velocity oblique (45°) to bedding.
$V_{P_{90}}$	P-wave velocity perpendicular to bedding.
V_P	P-wave velocity.
V_P/V_S	Ratio between compressional (P) and shear (S) wave velocities.
V_{S_0}	S-wave velocity normal to bedding.
$V_{S_{90}}$	S-wave velocity perpendicular to bedding.
V_S	S-wave velocity.
W_m	Energy stored.
E_{\Im}	Imaginary part of Young's modulus E .
E_{\Re}	Real part Young's modulus E .
G_{\Im}	Imaginary part of shear modulus G .
G_{\Re}	Real part of shear modulus G .
K_{\Im}	Imaginary part of bulk modulus K .
K_{\Re}	Real part of bulk modulus K .
Q_E	Quality-factor of Young's modulus E .
Q_G	Quality-factor of shear modulus G .
Q_K	Quality-factor of bulk modulus K .